Contributions of World Regions to the Global Tropospheric Ozone Burden Change from 1980 to 2010

Yuqiang Zhang[1], Jason West[2], Louisa K. Emmons[3], Kengo Sudo[4], Takashi Sekiya[5], Johannes Flemming[6], jan Eiof Jonson[7], and Marianne Tronstad Lund[8]

[1]Duke University
[2]University of North Carolina
[3]National Center for Atmospheric Research (UCAR)
[4]Nagoya University
[5]Japan Agency for Marine-Earth Science and Technology
[6]ECMWF
[7]Norwegian Meteorological Institute
[8]CICERO

November 21, 2022

Abstract

We investigate the contributions of emission changes from 10 world regions, as well as the global methane concentration change, on the global tropospheric ozone burden change from 1980 to 2010. The modeled global tropospheric ozone burden has increased by 28.1 Tg, with 26.7% (7.5 Tg) of this change attributed to the global methane increase. Southeast Asia (5.6 Tg) and South Asia (4.0) contribute comparably to the global ozone burden change as East Asia (5.6), even though NO emission increases in each region are less than one third of those in East Asia, highlighting the greater sensitivity of global ozone to these regions. Emission decreases from North America, Europe and Former Soviet Union have led to ozone burden decreases of 2.8, 1.0, and 0.3 Tg. The greater sensitivity of the global ozone burden to emission changes in tropical regions emphasizes the importance of controlling emissions in these regions for global ozone.

Contributions of World Regions to the Global Tropospheric Ozone Burden Change from 1980 to 2010

Yuqiang Zhang[1], J. Jason West[2], Louisa K. Emmons[3], Johannes Flemming[4], Jan Eiof Jonson[5], Marianne Tronstad Lund[6], Takashi Sekiya[7], Kengo Sudo[7]

[1]Nicholas School of the Environment, Duke University, 9 Circuit Dr, Durham, NC 27708, USA.

[2]Environmental Sciences and Engineering Department, University of North Carolina at Chapel Hill, Chapel Hill, North Carolina 27599, USA.

[3]Atmospheric Chemistry Observations and Modeling Laboratory, National Center for Atmospheric Research (NCAR), Boulder, CO, USA

[4]European Center for Medium-Range Weather Forecasts, Reading, UK

[5]Norwegian Meteorological Institute, Oslo, Norway

[6]CICERO Center for International Climate Research, Oslo, Norway

[7]Japan Agency for Marine-Earth Science and Technology, Yokohama, Japan

[8]Nagoya University, Furocho, Chigusa-ku, Nagoya, Japan

Corresponding author: Yuqiang Zhang (Yuqiang.Zhang@duke.edu)

Key Points:

- Tropospheric ozone burden increased from 1980 to 2010, driven mainly by increases in emissions from Southeast Asia, East Asia and South Asia, as well as global methane concentration increases;
- Among regions, greatest ozone burden influence came from Southeast Asia despite smaller emission increases, highlighting the much greater sensitivity for this region.

Abstract

We investigate the contributions of emission changes from 10 world regions, as well as the global methane concentration change, on the global tropospheric ozone burden change from 1980 to 2010. The modeled global tropospheric ozone burden has increased by 28.1 Tg, with 26.7% (7.5 Tg) of this change attributed to the global methane increase. Southeast Asia (5.6 Tg) and South Asia (4.0) contribute comparably to the global ozone burden change as East Asia (5.6), even though NO_x emission increases in each region are less than one third of those in East Asia, highlighting the greater sensitivity of global ozone to these regions. Emission decreases from North America, Europe and Former Soviet Union have led to ozone burden decreases of 2.8, 1.0, and 0.3 Tg. The greater sensitivity of the global ozone burden to emission changes in tropical and subtropical regions emphasizes the importance of controlling emissions in these regions for global ozone.

Plain Language Summary

The global tropospheric ozone burden is highly sensitive to emission changes in tropical and subtropical regions, due to high temperature, strong sunlight, and convection which are favorable for ozone production and accumulation. Through model sensitivity simulations, we show that emission increases in Southeast Asia, South Asia, and East Asia contribute over half of the global tropospheric ozone burden increase from 1980 to 2010. Southeast Asia and South Asia contribute about as much to the ozone increase as East Asia, even though emission increases were much smaller from these regions, showing the high ozone sensitivity in these regions.

1 Introduction

Ozone (O_3) at the surface is detrimental to human health, crop yields, and ecosystems (Silva et al., 2013; Zhang et al., 2018; Fowler et al., 2009; Cooper et al., 2014; Monks et al., 2015; Mills et al., 2018). Ozone in the troposphere is recognized as the third most important greenhouse gas, following carbon dioxide (CO_2) and methane (CH_4) (Myhre et al., 2013). Ozone is a secondary air pollutant, which is not emitted directly, but is produced through chemical reactions of precursor gases in the atmosphere, such as nitrogen oxides (NO_x), carbon monoxide (CO), CH_4, and non-methane volatile organic compounds (NMVOCs). O_3 precursors are mainly emitted by human activities, such as fossil fuel combustion, residential burning, oil and gas production, agriculture, and biomass burning. Observations from aircraft, ozonesondes, and different satellites show that the tropospheric ozone burden has been increasing second half of the 20th century (Gaudel et al., 2018; TF HTAP 2010). Both satellite ozone measurements and global chemical transport models have found that the largest ozone burden increases – about +6 to +7 Dobson units (i.e., ~15% to 20% of average background ozone) from 1980 to 2016 – are over India, Southeast Asia and East Asia (Ziemke et al., 2019).

Previous studies have demonstrated that methane emissions affect global ozone with little dependence on the location of emissions (Fiore et al., 2008). For short-lived ozone precursors, the global tropospheric ozone burden (B_{O3}) responds differently to emission changes from different world regions, with generally much greater sensitivity to emissions in tropical and subtropical regions (Naik et al., 2005; West et al., 2009a; Fry et al., 2012, 2013, and 2014). Since about 1980, global anthropogenic emissions of O_3 precursors have been shifting toward the equator, particularly decreasing in North America and Europe, and increasing in East and South Asia (Richter et al., 2005; Larmarque et al., 2010; Granier et al., 2011; Xing et al., 2013; Duncan et al.,

2016). In our previous study (Zhang et al., 2016), we investigated for the first time the influences of changes in the spatial distribution of global anthropogenic emissions of short-lived ozone precursors, the magnitude of these emissions, and the global atmospheric methane concentration on the global B_{O3} change from 1980 to 2010. We found that the spatial distribution change of emissions is most important for the increase in B_{O3}, slightly exceeding the combined influences of the increased emission magnitude and global methane (Zhang et al., 2016). We also found that B_{O3} has increased most strongly over Southeast, East, and South Asia, a conclusion that was supported by satellite and ozonesonde observations. Based on previous studies that found a much greater sensitivity of B_{O3} to emissions in tropical and subtropical regions and especially Southeast Asia, we hypothesized that emission increases from these regions were particularly important for the global B_{O3} increase, because of the strong sunlight, high temperature, and strong convection (Gupta et al., 1998; Lawrence et al., 2003; West et al., 2009a). However, the effects of emission changes over recent decades from individual world regions on the global B_{O3} has not been previously quantified.

Here we build on our previous study (Zhang et al., 2016) by investigating how emission changes from different world regions, as well as the global methane concentration changes, have contributed to global B_{O3} changes (ΔB_{O3}) from 1980 to 2010. We are particularly interested in quantifying the contributions of emissions from tropical and subtropical regions including Southeast Asia. We also calculate B_{O3} changes from multi-model experiments from the second phase of the Task Force on Hemispheric Transport of Air Pollutants (HTAP2, Galmarini et al., 2017), which have not been reported previously, to investigate the sensitivity of B_{O3} to emissions from different world regions.

2 Methods

The global chemistry–climate model CAM-chem is used in this study, which is based on the global Community Atmosphere Model (CAM) version 4, the atmospheric component of the Community Earth System Model (CESM, v1.2.2) (Larmarque et al., 2012; Tilmes et al., 2015, 2016). Model simulations are constructed to be consistent with those in our previous study (Zhang et al., 2016). The model uses a horizontal grid with a resolution of $2.5^o \times 1.9^o$ (longitude × latitude), and 56 vertical levels between the surface and 4 hPa (≈40 km) with a time step of 1800 s. The NASA Global Modeling and Assimilation Office GEOS-5 meteorology from 2008 to 2012 is used to drive the model as a chemical transport model, such that meteorological inputs for all simulations are identical. For all simulations, the first year is spin-up and results are presented as four-year averages. By using fixed meteorology, we focus on the effects of changes in anthropogenic emissions on B_{O3}, and ignore other influences, such as possible influences of climate change. Monthly mean distributions of chemically active stratospheric species (such as O_3, NO, NO_2 and N_2O_5) are prescribed using the climatology from the Whole Atmospheric Community Climate Model simulations (Garcia et al., 2007; Lamarque et al., 2012). Global anthropogenic emissions of all short-lived species including ozone precursors, aerosols, and aerosol precursors, from all anthropogenic sectors including biomass burning, are from ACCMIP for 1980 (Larmarque et al., 2010) and RCP8.5 for 2010 (Riahi et al., 2011), which are compatible with one another. Monthly temporal variations for the anthropogenic air pollutant emissions are added by using monthly emission factors from RETRO (Schultz et al., 2008) and the NMVOCs are re-speciated into CAM-chem chemical species following previous methods (Fry et al., 2014; Silva et al., 2016). All natural emissions, such as biogenic, lightning NO_x, volcano, soil NO_x, and

ocean emissions used the same configuration as in our previous study (Zhang et al., 2016; Lamarque et al., 2012), and are constant across all simulations.

We use three base simulations from our previous study (Zhang et al., 2016), the first two of which have global anthropogenic emissions and methane concentrations for 1980 (S_1980) and 2010 (S_2010), and a third in which CH_4 concentration is set to the 1980 level and all other parameters stay the same as S_2010 (named S_CH_4). In this study, we conduct another ten sensitivity simulations; for each of these, we replace the anthropogenic emissions of all air pollutants in 2010 with their emissions in 1980, for ten world regions individually, holding all other regions and the global CH_4 concentration at the 2010 levels (Table S1). The differences between S_2010 and the 10 sensitivity runs (S_2010 - sensitivity) are the ΔB_{O3} from that region's emission changes from 1980 to 2010. B_{O3} is defined as the total O_3 mass below the chemical tropopause of 150 ppbv ozone in the S_2010 simulation, with the same tropopause applied to all the other simulations.

The ten world regions follow the definitions introduced by HTAP2, except that we reduce the 13 land regions from HTAP2 to 10 regions here, grouping Northern Africa and Sub-Saharan together as a new region Africa (AFR), grouping Mexico and Central America and South America to give Central South America (CSA), and grouping Russia, and Belarus, Ukraine and Central Asia to give the Former Soviet Union (FSU). The other 7 regions include North America (NAM), Europe (EUR), South Asia (SAS), East Asia (EAS), South East Asia (SEA), Pacific, Australia and New Zealand (PAN), and the Middle East (MDE) (Figure S1). Since in HTAP2 definitions the region classification number for each grid cell is defined by the largest area fraction contributed by individual regions (Janssens-Maenhout et al., 2015), we found that when these region definitions are applied to ACCMIP and RCP8.5 emissions, some coastal cells with emissions were treated as ocean. To ensure we account for the relevant emissions from each region, we extend the 10 land mass regions outward into the oceans by two grid cells at 0.5º×0.5º horizontal resolution. By doing this, the inland region emissions increase by 2%-30% depending on the region and air pollutant, compared with the case when we do not include the two extra cells (Tables S2-S4 in the supporting information).

To evaluate model performance in simulating the surface, vertical and long-term O_3 trends from 1980 to 2010, we thoroughly compared the model results in S_1980 and S_2010 with long-term surface observations, ozonesonde, aircraft, and satellites in our previous work (Zhang et al., 2016). Compared with surface O_3 observations, S_2010 overestimates O_3 by 5.8 ppbv averaged over all stations in the US (average from 2009 to 2012 from the US CASTNET network), and 0.7 ppbv over Europe (average from 2009 to 2011 from the EMEP network), but captures the seasonal cycles very well. Our model also captures very well the vertical distribution of O_3 from ozonesondes, although it is biased high between 30ºS and 30ºN, particularly in the upper troposphere. The B_{O3} in 2010 (342.7±4.5 Tg yr^{-1}) simulated by CAM-Chem is in the range of multi-model simulations (ACCENT: 336 ± 27 Tg; ACCMIP: 337 ± 23 Tg; TOAR: 340 ± 34 Tg, and CMIP6: 348 ± 15 Tg (Young et al., 2013, 2018; Griffiths et al., 2020), and is also comparable with satellite observations (Ziemke et al., 2011, 2019). The estimated net increase of B_{O3} of about 28 Tg from 1980 to 2010 is also consistent with OMI/MLS satellite retrievals between October 2004 and December 2016, which indicate a 21.8 Tg increase in tropospheric ozone over 60ºS–60ºN (Blunden and Arndt, 2017).

3 Results

3.1 Regional emission changes

From 1980 to 2010, EAS had by far the largest NO_x emissions increase (16.6 Tg), triple the emissions in 1980, mainly from industry and transportation, as well as the largest increase in VOCs emissions (Fig 1 for absolute changes in Tg; Figs S2 and S3 for relative changes in %). The largest increases in CO emissions occurred in AFR (49.9 Tg, 22% higher than 1980, Fig. S2), EAS (47.0 Tg, 40%), and SAS (45.9 Tg, 70%), due to residential biomass burning and industrial emissions (Hoesly et al., 2018). SAS and SEA also have large emission increases for these pollutants. NAM and EUR had the largest emission decreases of 62% and 69% for CO, 36%, 32% for NO_x, and 67%, 47% for NMVOCs (Fig. S2). The overall decline of CO emissions likely resulted from motor vehicle emission controls (Granier et al., 2011; Hoesly et al., 2018), while the NO_x decreases were likely from the implementation of emission control devices on thermal power plants, the shuttering of inefficient plants, and stricter vehicle emission standards in these regions (Lamsal et al., 2015; Duncan et al., 2016). NO_x emissions in FSU have also decreased by 43%, but CO increased by 52% (Fig. S2), largely from residential emissions (Popovicheva et al., 2014; Hoesly et al., 2018).

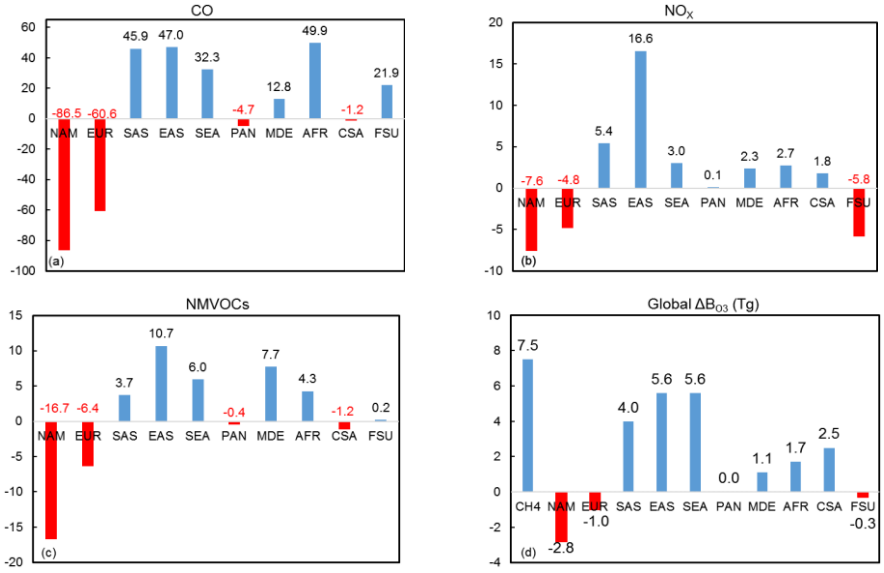

Figure 1. Emission changes from 1980 to 2010 for CO (a, Tg CO), NO_x (b, Tg NO_2), and NMVOCs (c, Tg NMVOCs), and global tropospheric ozone burden changes (d, Tg O_3) from global methane increases as well as emission changes from the 10 world regions.

3.2 Global tropospheric ozone changes

The global B_{O3} is modeled to have increased 28.1 Tg from 1980 to 2010, with the largest increase from the global CH_4 increase (7.5 Tg, Fig. 1d). Among the 10 regions, the global ΔB_{O3} is estimated to increase most from emission changes in SEA (5.6 Tg), EAS (5.6 Tg) and SAS (4.0 Tg). These three regions together accounted for 54% of the global ΔB_{O3}. Emission decreases from NAM and EUR contributed ΔB_{O3} decreases of -2.8 Tg and -1.0 Tg (Fig. 1d). Emission changes in FSU also contributed global ΔB_{O3} decreases (-0.3 Tg), mainly caused by the NO_x decreases (Fig. 1d). Other regions contributed to the global ΔB_{O3} from negligibly (~0 Tg fom PAN) to considerably (2.5 Tg from CSA). The total global ΔB_{O3} summed from the global CH_4

concentration change and the emission changes in the 10 world regions (23.9 Tg) are slightly lower than difference between S_2010 and S_1980 (28.1 Tg), mainly because of the nonlinear response of ozone to the precursors, but also because we do not account for emission changes over the oceans (Tables S2-S4). Although EAS has much larger NO_x and NMVOCs increases from 1980 to 2010 than that in SAS and SEA (Fig. 1), the ΔB_{O3} are comparable between these three regions, as a result of the large sensitivity of ΔB_{O3} to NO_x emissions in SAS and SEA (Naik et al., 2005; West et al., 2009a; Fry et al., 2012).

The spatial pattern of the modeled ΔB_{O3} also suggests a strong influence of emission increases from SEA, EAS, and SAS, and decreases from NAM and EUR, and this pattern is consistent with satellite observations (Ziemke et al., 2019). The global CH_4 concentration increase has contributed more uniformly to the global ΔB_{O3} (Fig. 2b), but does not explain the pattern of ΔB_{O3}.

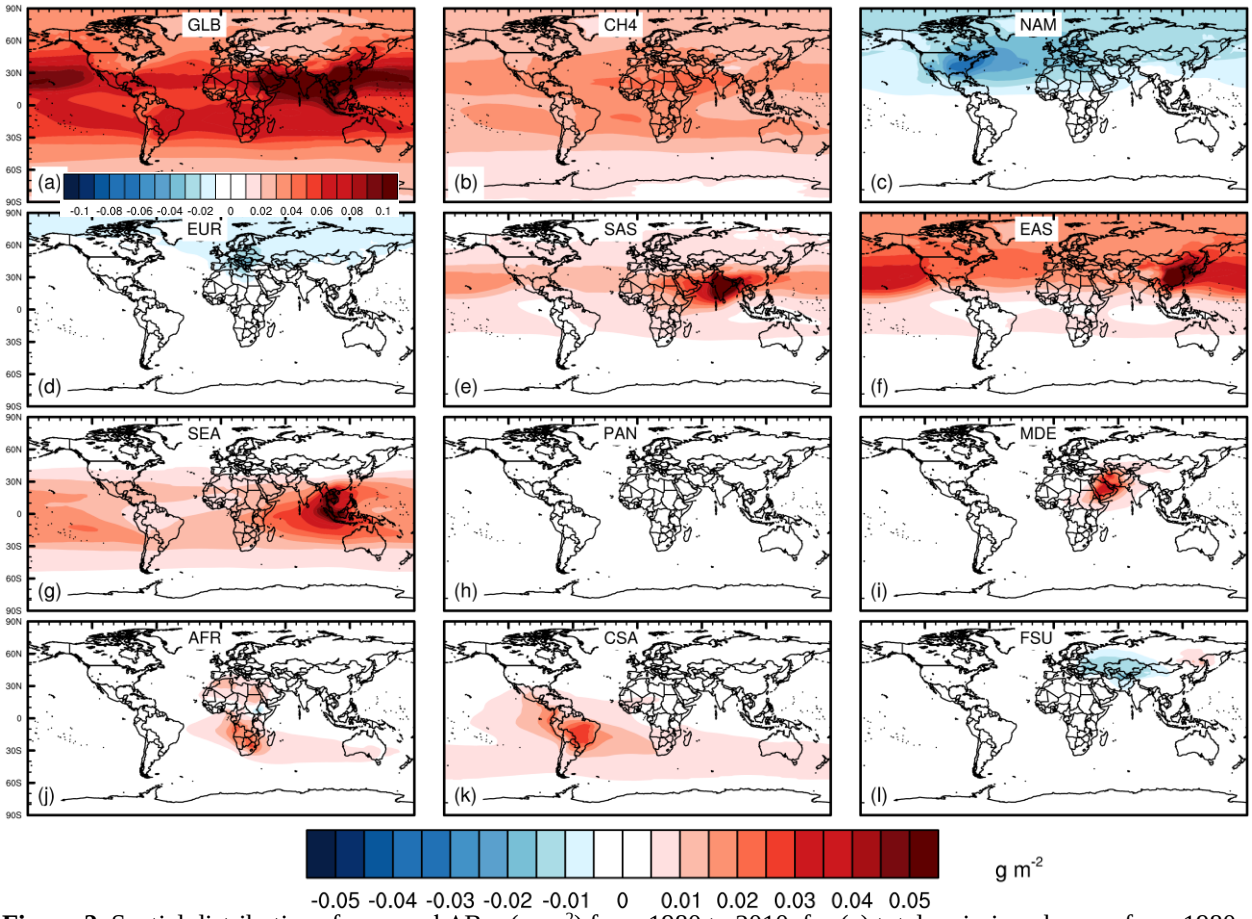

Figure 2. Spatial distributions for annual ΔB_{O3} (g m^{-2}) from 1980 to 2010, for (a) total emission changes from 1980 to 2010, (b) global CH_4 concentration change, and (c)-(l) emission changes in 10 world regions. Note the different colorbar used in panel a.

The global zonal ΔB_{O3} increases are more notable in the northern hemisphere (NH) than that in the southern hemisphere (SH) extending from the surface to 100 hPa (Fig. 3). The global zonal ΔB_{O3} increases show a strong influence of global CH_4, which is more spatially uniform than in the regional scenarios. Emission increases from SEA and SAS cause large ozone increases over the tropics, extending to high elevation, which shows the strong convection over these regions. This convection lifts ozone precursors to high elevations where they have a longer lifetime to form

and accumulate ozone, reflecting the higher temperature and strong sunlight in these regions (Lawrence et al., 2003; Zhang et al., 2016). Although the tropics have greater water vapor, which causes greater HO_x radicals that destroy ozone, less HO_x is likely present at higher elevation, and the ozone lifetime would be longer. In contrast, ozone reductions over NAM and EUR stay at high latitude, with little transport toward the equator, and do not reach high altitude. Much of the emissions from EAS are far enough north that they are mainly not transported toward the equator, or to high altitude, helping to explain the lower sensitivity for emissions from EAS relative to SEA and SAS.

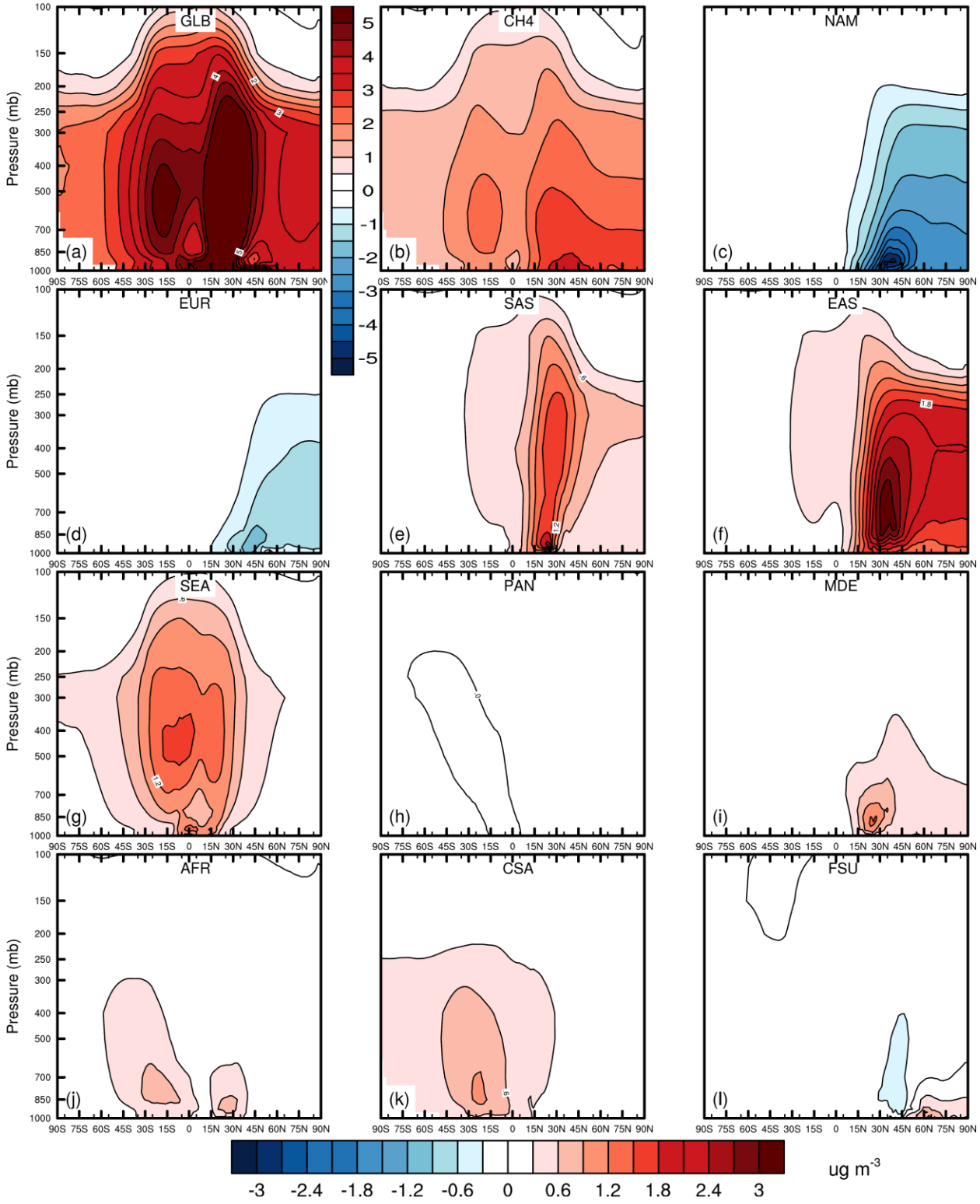

Figure 3. Zonal annual average O_3 change (μg m^{-3}) from 1980 to 2010, for (a) total emission changes, (b) global CH_4 concentration change, and (c)-(l) emission changes in 10 world regions. Note the different colorbar used in panel a.

We also analyzed spatial and zonal ΔB_{O3} in each season (Figs. S4 to S12). In JJA and SON, there is greater sensitivity to emissions from EAS and SAS, as the intertropical convergence zone is further north, and emissions from EAS and SAS are transported more effectively toward the tropics and high elevation. In contrast, emissions from SEA do not cause large differences in B_{O3} in different seasons. NAM and EUR have slightly larger ΔB_{O3} decreases in JJA (Fig. S8).

3.3 Comparisons with HTAP2 sensitivity experiments

To further investigate the greater sensitivity of ΔB_{O3} to emissions from tropical and subtropical regions, we calculated the global ΔB_{O3} for regional reductions from the HTAP2 multimodel experiment, which simulated 2010. Previous HTAP2 studies have analyzed regional emission perturbations on surface air quality and radiative forcing changes, but here we present ΔB_{O3} for experiments which simulated 20% reductions in all anthropogenic air pollutant emissions globally and from six source regions analyzed here: NAM, EUR, SAS, EAS, RBU (here RBU in the HTAP2 experiment equivalent to the FSU region in our study), and MDE (Janssens-Maenhout et al., 2015; Stjern et al., 2016; Galmarini et al., 2017). We chose to analyze the six CTMs (Table S5) that simulated the base experiment, the global 20% reduction, and the 20% reductions from at least four of six regions.

Whereas the HTAP2 experiments reduced emissions of multiple precursors by the same percentage, our experiments changed emissions by different percentages for different precursors based on the changes from 1980 to 2010. To compare the modeled sensitivities, we normalize the global ΔB_{O3} by the NO_x emission changes (Tg O_3 / (Tg N yr^{-1})), since previous studies found that percent changes in NO_x produce greater B_{O3} changes compared with CO and NMVOCs (Fry et al., 2012). For HTAP2 experiments, the global ΔB_{O3} (Fig. S13) is most sensitive to changes in emissions from SAS and MDE (Fig. 4). In our experiments, SAS and MDE also had the greatest sensitivities of the six regions that HTAP2 studies by perturbing emissions. However, we also find that the highest sensitivities occur in three regions that HTAP2 did not simulate, and which are mainly in tropical and subtropical regions – SEA (6.1 Tg O_3 / (Tg N yr^{-1}), CSA (4.7) and PAN (3.7) – and we also show high sensitivity to emissions from AFR. The HTAP2 results for SAS and MDE provide supportive evidence for our conclusion of greater sensitivity from tropical and subtropical regions, suggesting that future experiments analyzing ozone like HTAP2 should include more regions and give a greater priority to studying the impact of emissions from the tropics. From Fig. 4, we also see that the global ΔB_{O3} sensitivity to 20% global emission perturbations (GLO) is lower (ensemble mean of 1.5 Tg O_3 / (Tg N yr^{-1})) than that in our study (3.1 Tg O_3 / (Tg N yr^{-1})), mostly caused by the different percent changes of other air pollutants (CO and NMVOCs).

(a)

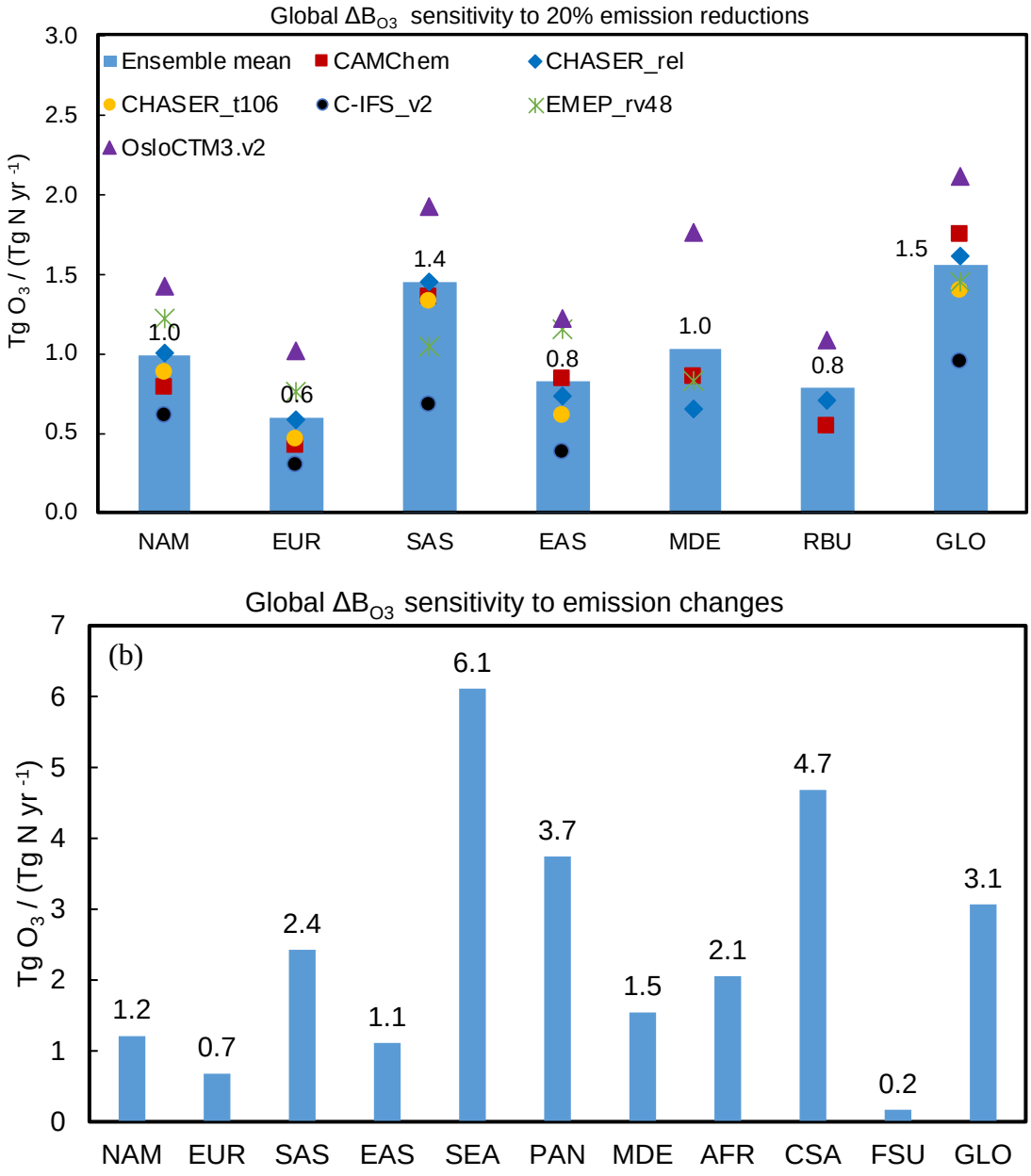

Figure 4. The sensitivity of global tropospheric ozone burden changes, normalized per unit NO_x emissions, to (a) regional and global 20% emission reductions in 2010 for all anthropogenic air pollutants from the HTAP2 experiments (blue columns are the ensemble mean from the 6 models), (b) regional and global emission changes from 1980 to 2010 in all anthropogenic air pollutants (unit of Tg O_3 / (Tg N yr^{-1})). Note for the HTAP2 results in panel a, the CHASER_t106 and C-IFS_v2 models did not perform the MDE and RBU perturbation experiments, and the EMEP_rv48 model did not perform the RBU experiment. In Fig b, for the GLO (3.1 Tg O_3/ (Tg N yr^{-1})) we do not consider the B_{O3} changes caused by CH_4 concentration changes from 1980 to 2010 (S_CH_4 – S_1980), to compare with the HTAP2 results.

4 Conclusions and Discussion

The global ozone burden is modeled to have increased from 1980 to 2010 by 28.1 Tg, with global CH_4 concentration increases contributing 26.7% of this total (7.5 Tg). Among world regions, emission increases in Southeast Asia (5.6 Tg), East Asia (5.6 Tg), and South Asia (4.0

Tg) are most important for the global ozone burden, together accounting for 54% of the total change. East Asia has much larger NO_x and NMVOCs increases from 1980 to 2010 than those in Southeast Asia and South Asia, but the global ozone burden change is comparable between these three regions, as a result of large strong sensitivity of ozone burden and convection over these tropical and subtropical regions. The emission reductions in North America and Europe contribute to global ozone burden decreases, by 2.8 Tg and 1.0 Tg. We further calculate the sensitivity of ΔB_{O3} to regional emission from the HTAP2 multimodel experiment, which also simulated 2010. From HTAP2 experiments, we find that the global ΔBO_3 also has large sensitivity to changes in emissions from SAS and MDE regions (the HTAP2 experiments did not simiulate perturbations from SEA), consistent with our findings.

Changes in emissions of NO_x, VOCs, and CO affect concentrations of the hydroxyl radical (OH), which is the major sink for CH_4 (Wang and Jacob, 1998; Wild and Prather, 2000; Fiore et al., 2002). The changes in CH_4 lifetime are important for climate forcing and in turn affect global tropospheric ozone concentration in the long-term (West et al., 2007; West et al., 2009b; Stevenson et al., 2006, 2013). We did not include this long-term ozone influence, since simulations used observed CH_4 concentrations in 1980 and 2010. But changes in ozone precursor emissions from different world regions affected this growth of methane. Future work should model the effects of historic changes in ozone precursors from different world regions on methane and long-term ozone via changes in OH.

We conclude that special attention should be paid in both research and environmental policy to low latitude regions, such as Southeast Asia and South Asia because of the greater sensitivity of the global tropospheric ozone burden. NO_x emissions from these two regions increased only 18% and 33% of the NO_x increases in East Asia from 1980 to 2010, but their effects on the global ozone burden are comparable. Since 2010, global emissions have continued to evolve, as China is now reducing emissions (Li M. et al., 2017 2018; Zheng et al., 2018a,b). However, ozone concentrations have worsened recently in China and it remains an important issue (Lu et al., 2018, 2020). Meanwhile, emissions in India and other South Asia regions have continued to grow (Li C. et al., 2017; Koplitz et al., 2017; Kumar et al., 2018), and emissions from Africa are expected to accelerate (Liousse et al., 2014). For example, emissions of CO, NO_x, and NMVOCs in South Asia are projected to increase by 116%, 6%, and 18% in 2050 under the RCP8.5 scenario, and 72%, 4%, and 12% under the RCP6.0 scenario, relative to 2000 (Kumar et al., 2018). The global shift of emissions toward the equator, where global ozone sensitivity is greater, is therefore expected to continue. More efforts to reduce ozone precursor emissions domestically and internationally, including through methane reductions (West et al., 2006), are therefore needed to combat ozone as global issue.

Acknowledgments

Y. Zhang is supported by NASA Grant #NNX15AL2, and J.J. West is supported by EPA STAR (#RD83587801) and NASA (#NNX16AQ30G). We would like to thank the University of North Carolina at Chapel Hill Research Computing group for providing computational resources and support that have contributed to these research results. The National Center for Atmospheric Research (NCAR) is funded by the National Science Foundation. Datasets for the HTAP2 multi-model results used in this research are available through the AeroCom servers (http://aerocom.met.no/data.html, accessed 2020-07-23, Labonne et al., 2017).

References

Blunden, J. and Arndt, D. S. Eds., (2017). State of the Climate in 2016. Bull. Amer. Meteor. Soc., 98 (8), Si–S277, doi:10.1175/2017BAMSStateoftheClimate.1.

Cooper, O. R., Parrish, D. D., Ziemke, J., Balashov, N. V., Cupeiro, M., Galbally, I. E., et al. (2014). Global distribution and trends of tropospheric ozone: An observation-based review. *Elementa: Science of the Anthropocene*, *2*, 000029. https://doi.org/10.12952/journal.elementa.000029

Duncan, B. N., Lamsal, L. N., Thompson, A. M., Yoshida, Y., Lu, Z., Streets, D. G., et al. (2016). A space-based, high-resolution view of notable changes in urban NO_x pollution around the world (2005–2014). *Journal of Geophysical Research Atmospheres*, *121*(2), 976–996. https://doi.org/10.1002/2015JD024121

Fiore, A. M., J. J. West, L. W. Horowitz, V. Naik, and M. D. Schwarzkopf (2008) Characterizing the tropospheric ozone response to methane emission controls and the benefits to climate and air quality, *Journal of Geophysical Research*, 113: D08307, 16 p., doi: 10.1029/2007JD009162.

Fry, M. M., Naik, V., West, J. J., Schwarzkopf, M. D., Fiore, A. M., Collins, W. J., et al. (2012). The influence of ozone precursor emissions from four world regions on tropospheric composition and radiative climate forcing. *Journal of Geophysical Research: Atmospheres*, *117*, D07306. https://doi.org/10.1029/2011JD017134

Fry, M. M., Schwarzkopf, M. D., Adelman, Z., Naik, V., Collins, W. J., & West, J. J. (2013). Net radiative forcing and air quality responses to regional CO emission reductions. *Atmospheric Chemistry and Physics*, *13*, 5381–5399. https://doi.org/10.5194/acp-13-5381-2013.

Fry, M. M., Schwarzkopf, M. D., Adelman, Z., & West, J. J. (2014). Air quality and radiative forcing impacts of anthropogenic volatile organic compound emissions from ten world regions. *Atmospheric Chemistry and Physics*, *14*, 523–535. https://doi.org/10.5194/acp-14-523-2014.

Fowler, D., Pilegaard, K., Sutton, M. A., Ambus, P., Raivonen, M., Duyzer, J., et al. (2009). Atmospheric composition change: Ecosystems-Atmosphere interactions. *Atmospheric Environment*, *43*(33), 5193–5267. https://doi.org/10.1016/j.atmosenv.2009.07.068.

Galmarini, S., Koffi, B., Solazzo, E., Keating, T., Hogrefe, C., Schulz, M., et al. (2017). Technical note: Coordination and harmonization of the multi-scale, multi-model activities HTAP2, AQMEII3, and MICS-Asia3: Simulations, emission inventories, boundary conditions, and model output formats. *Atmospheric Chemistry and Physics*, *17*(2), 1543–1555. https://doi.org/10.5194/acp-17-1543-2017.

Garcia, R. R., Marsh, D. R., Kinnison, D. E., Boville, B. A., & Sassi, F. (2007). Simulation of secular trends in the middle atmosphere, 1950-2003. *Journal of Geophysical Research: Atmospheres*, *112*, D09301. https://doi.org/10.1029/2006JD007485.

Gaudel, A., Cooper, O. R., Ancellet, G., Barret, B., Boynard, A., Burrows, J. P., et al. (2018). Tropospheric Ozone Assessment Report: Present-day distribution and trends of tropospheric ozone relevant to climate and global atmospheric chemistry model evaluation. *Elem Sci Anth*, *6*. https://doi.org/10.1525/elementa.291.

Granier, C., Bessagnet, B., Bond, T., D'Angiola, A., Denier van der Gon, H., Frost, G. J., et al. (2011). Evolution of anthropogenic and biomass burning emissions of air pollutants at global and regional scales during the 1980–2010 period. *Climatic Change*, *109*(1–2), 163–190. https://doi.org/10.1007/s10584-011-0154-1.

Griffiths, P. T., Murray, L. T., Zeng, G., Archibald, A. T., Emmons, L. K., Galbally, I., et al. (2020) Tropospheric ozone in CMIP6 Simulations, Atmos. Chem. Phys. Discuss., https://doi.org/10.5194/acp-2019-1216.

Guenther, A. B., Jiang, X., Heald, C. L., Sakulyanontvittaya, T., Duhl, T., Emmons, L. K., & Wang, X. (2012). The model of emissions of gases and aerosols from nature version 2.1 (MEGAN2.1): An extended and updated framework for modeling biogenic emissions. *Geoscientific Model Development*, *5*, 1471–1492. https://doi.org/10.5194/gmd-5-1471-2012

Gupta, M. L., Cicerone, R. J., & Elliott, S. (1998). Perturbation to global tropospheric oxidizing capacity due to latitudinal redistribution of surface sources of NO_x, CH_4 and CO. *Geophysical Research Letters*, *25*(21), 3931–3934.

Hoesly, R. M., Pitkanen, T., Vu, L., Kurokawa, J., Janssens-Maenhout, G., Andres, R. J., et al. (2018). Historical (1750-2014) anthropogenic emissions of reactive gases and aerosols from the Community Emission Data System (CEDS). *Geoscientific Model Development*, *11*(1), 369–408,. https://doi.org/https://doi.org/10.5194/gmd-11-369-2018

Janssens-Maenhout, G., Crippa, M., Guizzardi, D., Dentener, F., Muntean, M., Pouliot, G., et al. (2015). HTAP-v2.2: A mosaic of regional and global emission grid maps for 2008 and 2010 to study hemispheric transport of air pollution. *Atmospheric Chemistry and Physics*, *15*(19), 11411–11432. https://doi.org/10.5194/acp-15-11411-2015

Koplitz, S. N., Jacob, D. J., Sulprizio, M. P., Myllyvirta, L., & Reid, C. (2017). Burden of Disease from Rising Coal-Fired Power Plant Emissions in Southeast Asia. *Environmental Science and Technology*, *51*(3), 1467–1476. https://doi.org/10.1021/acs.est.6b03731

Kumar, R., Barth, M. C., Pfister, G. G., Delle Monache, L., Lamarque, J. F., Archer-Nicholls, S., et al. (2018). How Will Air Quality Change in South Asia by 2050? *Journal of Geophysical Research: Atmospheres*, *123*(3), 1840–1864. https://doi.org/10.1002/2017JD027357

Lamarque, J.-F., Bond, T. C., Eyring, V., Granier, C., Heil, A., Klimont, Z., et al. (2010). Historical (1850-2000) gridded anthropogenic and biomass burning emissions of reactive gases and aerosols: Methodology and application. *Atmospheric Chemistry and Physics*, *10*, 7017–7039. https://doi.org/10.5194/acp-10-7017-2010

Lamarque, J.-F., Emmons, L. K., Hess, P. G., Kinnison, D. E., Tilmes, S., Vitt, F., et al. (2012). CAM-chem: description and evaluation of interactive atmospheric chemistry in the Community Earth System Model. *Geoscientific Model Development*, *5*, 369–411. https://doi.org/10.5194/gmd-5-369-2012

Lamsal, L. N., Duncan, B. N., Yoshida, Y., Krotkov, N. A., Pickering, K. E., Streets, D. G., & Lu, Z. (2015). U.S. NO_2 trends (2005-2013): EPA Air Quality System (AQS) data versus improved observations from the Ozone Monitoring Instrument (OMI). *Atmospheric Environment*, *110*(2), 130–143. https://doi.org/10.1016/j.atmosenv.2015.03.055

Lawrence, M. G., Rolf, von K., Salzmann, M., & Rasch, P. J. (2003). The balance of effects of deep convective mixing on tropospheric ozone. *Geophysical Research Letters*, *30*(18), 3–6. https://doi.org/10.1029/2003GL017644

Labonne, M., Breon, F. M., & Schulz, M. (2017) AeroCom Database, AEROCOM, available at: http://aerocom.met.no/data.html (accessible upon request), last access: July 2020.

Li, C., McLinden, C., Fioletov, V., Krotkov, N., Carn, S., Joiner, J., et al. (2017). India Is Overtaking China as the World's Largest Emitter of Anthropogenic Sulfur Dioxide. *Scientific Reports*, *7*(1), 1–7. https://doi.org/10.1038/s41598-017-14639-8

Li, K., Jacob, D. J., Zhang, Q., Liao, H., Bates, K. H., & Shen, L. (2019). Anthropogenic drivers of 2013–2017 trends in summer surface ozone in China. *Proceedings of the National Academy of Sciences*, *116*(2), 422–427. https://doi.org/10.1073/pnas.1812168116

Li, M., Liu, H., Geng, G., Hong, C., Liu, F., Song, Y., et al. (2017). Anthropogenic emission inventories in China: A review. *National Science Review*, *4*(6), 834–866. https://doi.org/10.1093/nsr/nwx150

Li, M., Klimont, Z., Zhang, Q., Martin, R. V., Zheng, B., Heyes, C., et al. (2018). Comparison and evaluation of anthropogenic emissions of SO_2 and NO_x over China. *Atmospheric Chemistry and Physics*, *18*(5), 3433–3456. https://doi.org/10.5194/acp-18-3433-2018

Liousse, C., Assamoi, E., Criqui, P., Granier, C., & Rosset, R. (2014). Explosive growth in African combustion emissions from 2005 to 2030. *Environmental Research Letters*, *9*(3). https://doi.org/10.1088/1748-9326/9/3/035003

Lu, X., Hong, J., Zhang, L., Cooper, O. R., Schultz, M. G., Xu, X., et al. (2018). Severe Surface Ozone Pollution in China: A Global Perspective. *Environmental Science and Technology Letters*, *5*(8), 487–494. https://doi.org/10.1021/acs.estlett.8b00366

Lu, X., Zhang, L., Wang, X., Gao, M., Li, K., Zhang, Y., et al. (2020). Rapid Increases in Warm-Season Surface Ozone and Resulting Health Impact in China Since 2013. *Environmental Science & Technology Letters*. https://doi.org/10.1021/acs.estlett.0c00171

Mills, G., Pleijel, H., Malley, C. S., Sinha, B., Cooper, O. R., Schultz, M. G., et al. (2018). Tropospheric Ozone Assessment Report: Present-day tropospheric ozone distribution and trends relevant to vegetation. *Elem Sci Anth*, *6*(1), 47. https://doi.org/10.1525/elementa.302

Monks, P. S., Archibald, A. T., Colette, A., Cooper, O., Coyle, M., Derwent, R., et al. (2015). Tropospheric ozone and its precursors from the urban to the global scale from air quality to short-lived climate forcer. *Atmospheric Chemistry and Physics*, *15*(15), 8889–8973. https://doi.org/10.5194/acp-15-8889-2015.

Myhre, G., Shindell, D., Bréon, F.-M., Collins, W., Fuglestvedt, J., Huang, J., et al. (2013): Anthropogenic and Natural Radiative Forcing. In: Climate Change 2013: The Physical Science Basis. Contribution of Working Group I to the Fifth Assessment Report of the Intergovernmental Panel on Climate Change [Stocker, T.F., D. Qin, G.-K. Plattner, M. Tignor, S.K. Allen, J. Boschung, A. Nauels, Y. Xia, V. Bex and P.M. Midgley (eds.)]. Cambridge University Press, Cambridge, United Kingdom and New York, NY, USA.

Naik, V., Mauzerall, D., Horowitz, L., Schwarzkopf, M. D., Ramaswamy, V., & Oppenheimer, M. (2005). Net radiative forcing due to changes in regional emissions of tropospheric ozone precursors. *Journal of Geophysical Research: Atmospheres*, *110*, D24306. https://doi.org/10.1029/2005JD005908.

Prather, M., G. Flato, P. Friedlingstein, C. Jones, J.-F. Lamarque, H. Liao and P. Rasch (eds. 2013). Climate Change 2013: The Physical Science Basis. Contribution of Working Group I to the Fifth Assessment Report of the Intergovernmental Panel on Climate Change [eds Stocker, T. F. et al.], Annex II: Climate System Scenario Tables. *Cambridge University Press, Cambridge, United Kingdom and New York, NY, USA*, pp. 1395–1446, doi: 10.1017/CBO9781107415324.030.

Popovicheva, O., Kistler, M., Kireeva, E., Persiantseva, N., Timofeev, M., Kopeikin, V., & Kasper-Giebl, A. (2014). Physicochemical characterization of smoke aerosol during large-scale wildfires: Extreme event of August 2010 in Moscow. *Atmospheric Environment*, *96*, (October 2014), 405–414. https://doi.org/10.1016/j.atmosenv.2014.03.026.

Riahi, K., Rao, S., Krey, V., Cho, C., Chirkov, V., Fischer, G., et al. (2011). RCP 8.5-A scenario of comparatively high greenhouse gas emissions. *Climatic Change*, *109*(1), 33–57. https://doi.org/10.1007/s10584-011-0149-y.

Richter, A., Burrows, J. P., Nüß, H., Granier, C., & Niemeier, U. (2005). Increase in tropospheric nitrogen dioxide over China observed from space. *Nature*, *437*(7055), 129–132. https://doi.org/10.1038/nature04092.

Schultz, M.G., Backman, L., Balkanski, Y., Bjoerndalsaeter, S., Brand, R., Burrows. J.P., et al. (2008) REanalysis of the TROpospheric chemical composition over the past 40 years (RETRO) — A long-term global modeling study of tropospheric chemistry Final ReportJülich/Hamburg, Germany, August 2007.

Silva, R. A., West, J. J., Zhang, Y., Anenberg, S. C., Lamarque, J.-F., Shindell, D. T., et al. (2013). Global premature mortality due to anthropogenic outdoor air pollution and the contribution of past climate change. *Environmental Research Letters*, *8*, 034005. https://doi.org/10.1088/1748-9326/8/3/034005

Silva, R. A., Adelman, Z., Fry, M. M., & West, J. J. (2016). The impact of individual anthropogenic emissions sectors on the global burden of human mortality due to ambient air pollution. *Environmental Health Perspectives*, *124*(11), 1776–1784. https://doi.org/10.1289/EHP177

Spracklen, D. V., Logan, J. A., Mickley, L. J., Park, R. J., Yevich, R., Westerling, A. L., & Jaffe, D. A. (2007). Wildfires drive interannual variability of organic carbon aerosol in the western U.S. in summer. *Geophysical Research Letters*, *34*(16), 2–5. https://doi.org/10.1029/2007GL030037.

Stevenson, D. S., Dentener, F. J., Schultz, M. G., Ellingsen, K., van Noije, T. P. C., Wild, O., et al. (2006). Multimodel ensemble simulations of present-day and near-future tropospheric ozone. *Journal of Geophysical Research: Atmospheres*, *111*, D08301. https://doi.org/10.1029/2005JD006338.

Stevenson, D. S., Young, P. J., Naik, V., Lamarque, J. F., Shindell, D. T., Voulgarakis, A., et al. (2013). Tropospheric ozone changes, radiative forcing and attribution to emissions in the Atmospheric Chemistry and Climate Model Intercomparison Project (ACCMIP). *Atmospheric Chemistry and Physics*, *13*(6), 3063–3085. https://doi.org/10.5194/acp-13-3063-2013.

Stjern, C. W., Bjørn Hallvard Samset, G. M., Bian, H., Chin, M., Yanko Davila, Dentener, F., et al. (2016). Global and regional radiative forcing from 20% reductions in BC, OC and SO_4 – an HTAP2 multi-model study. *Atmospheric Chemistry and Physics*, *16*(21), 13579–13599. https://doi.org/10.5194/acp-16-13579-2016

TF HTAP: Hemispheric transport of air pollution, Part A: Ozone and partuculate matter, edited by: Frank Dentener, Terry Keating, and Hajime Akimoto, available at: http://www.htap.org/publications/2010_report/2010_Final_Report/HTAP2010PartA110407.pdf (last access: 21 June 2020), 2010.

Tilmes, S., Lamarque, J.-F., Emmons, L. K., Kinnison, D. E., Ma, P.-L., Liu, X., et al. (2015). Description and evaluation of tropospheric chemistry and aerosols in the Community Earth System Model (CESM1.2). *Geoscientific Model Development*, *8*(5), 1395–1426. https://doi.org/10.5194/gmd-8-1395-2015

Tilmes, S., Lamarque, J. F., Emmons, L. K., Kinnison, D. E., Marsh, D., Garcia, R. R., et al. (2016). Representation of the Community Earth System Model (CESM1) CAM4-chem

497 within the Chemistry-Climate Model Initiative (CCMI). *Geoscientific Model Development*,
498 *9*(5), 1853–1890. https://doi.org/10.5194/gmd-9-1853-2016
499 Wang, Y., & Jacob, D. J. (1998). Anthropogenic forcing on tropospheric ozone and OH since
500 preindustrial times. *Journal of Geophysical Research Atmospheres*, *103*(D23), 31123–
501 31135. https://doi.org/10.1029/1998JD100004
502 West, J. J., A. M. Fiore, L. W. Horowitz, and D. L. Mauzerall (2006) Global health benefits of
503 mitigating ozone pollution with methane emission controls, *Proceedings of the National*
504 *Academy of Sciences*, 103(11): 3988-3993, https://doi.org/10.1073/pnas.0600201103.
505 West, J. J., Fiore, A. M., Naik, V., Horowitz, L. W., Schwarzkopf, M. D., & Mauzerall, D. L.
506 (2007). Ozone air quality and radiative forcing consequences of changes in ozone precursor
507 emissions. *Geophysical Research Letters*, *34*(6), 1–5.
508 https://doi.org/10.1029/2006GL029173
509 West, J. J., Naik, V., Horowitz, L. W., & Fiore, A. M. (2009a). Effect of regional precursor
510 emission controls on long-range ozone transport – Part 1: Short-term changes in.
511 *Atmospheric Chemistry and Physics*, *9*, 6077–6093. https://doi.org/10.5194/acpd-9-7079-
512 2009
513 West, J. J., Naik, V., Horowitz, L. W., & Fiore, A. M. (2009b). Effect of regional precursor
514 emission controls on long-range ozone transport – Part 2: Steady-state changes in ozone air
515 quality and impacts on human mortality. *Atmospheric Chemistry and Physics*, *9*(16), 6095–
516 6107. https://doi.org/10.5194/acp-9-6095-2009
517 West, J. J., Smith, S. J., Silva, R. A., Naik, V., Zhang, Y., Adelman, Z., et al. (2013). Co-benefits
518 of Global Greenhouse Gas Mitigation for Future Air Quality and Human Health. *Nature*
519 *Climate Change*, *3*(10), 885–889. https://doi.org/10.1038/NCLIMATE2009
520 Wild, O., & Prather, M. J. (2000). Excitation of the primary tropospheric chemical mode in a
521 global three-dimensional model. *Journal of Geophysical Research Atmospheres*, *105*(D20),
522 24647–24660. https://doi.org/10.1029/2000JD900399
523 Xing, J., Pleim, J., Mathur, R., Pouliot, G., Hogrefe, C., Gan, C. M., & Wei, C. (2013). Historical
524 gaseous and primary aerosol emissions in the United States from 1990 to 2010. *Atmospheric*
525 *Chemistry and Physics*, *13*(15), 7531–7549. https://doi.org/10.5194/acp-13-7531-2013
526 Young, P. J., Archibald, A. T., Bowman, K. W., Lamarque, J.-F., Naik, V., Stevenson, D. S., et
527 al. (2013). Pre-industrial to end 21st century projections of tropospheric ozone from the
528 Atmospheric Chemistry and Climate Model Intercomparison Project (ACCMIP).
529 *Atmospheric Chemistry and Physics*, *13*, 2063–2090. https://doi.org/10.5194/acp-13-2063-
530 2013
531 Young, P. J., Naik, V., Fiore, A. M., Gaudel, A., Guo, J., Lin, M. Y., et al. (2018). Tropospheric
532 Ozone Assessment Report: Assessment of global-scale model performance for global and
533 regional ozone distributions, variability, and trends. *Elem Sci Anth*, *6*(1), 10.
534 https://doi.org/10.1525/elementa.265
535 Zhang, Y., Cooper, O. R., Gaudel, A., Thompson, A. M., Nédélec, P., Ogino, S. Y., & West, J. J.
536 (2016). Tropospheric ozone change from 1980 to 2010 dominated by equatorward
537 redistribution of emissions. *Nature Geoscience*, *9*(12), 875–879.
538 https://doi.org/10.1038/ngeo2827
539 Zheng, B., Chevallier, F., Ciais, P., Yin, Y., Deeter, M. N., Worden, H. M., et al. (2018a). Rapid
540 decline in carbon monoxide emissions and export from East Asia between years 2005 and
541 2016. *Environmental Research Letters*, *13*(4). https://doi.org/10.1088/1748-9326/aab2b3

Zheng, B., Tong, D., Li, M., Liu, F., Hong, C., Geng, G., et al. (2018b). Trends in China's anthropogenic emissions since 2010 as the consequence of clean air actions. *Atmospheric Chemistry and Physics*, *18*(19), 14095–14111. https://doi.org/10.5194/acp-18-14095-2018

Zheng, Y., Xue, T., Zhang, Q., Geng, G., Tong, D., Li, X., & He, K. (2017). Air quality improvements and health benefits from China's clean air action since 2013. *Environmental Research Letters*, *12*(114020). https://doi.org/https://doi.org/10.1088/1748-9326/aa8a32

Ziemke, J. R., Chandra, S., Labow, G. J., Bhartia, P. K., Froidevaux, L., & Witte, J. C. (2011). A global climatology of tropospheric and stratospheric ozone derived from Aura OMI and MLS measurements. *Atmospheric Chemistry and Physics*, *11*(17), 9237–9251. https://doi.org/10.5194/acp-11-9237-2011

Ziemke, J. R., Oman, L. D., Strode, S. A., Douglass, A. R., Olsen, M. A., McPeters, R. D., et al. (2019). Trends in Global Tropospheric Ozone Inferred from a Composite Record of TOMS/OMI/MLS/OMPS Satellite Measurements and the MERRA-2 GMI Simulation. *Atmospheric Chemistry and Physics*, *19*(5), 3257–3269. https://doi.org/https://doi.org/10.5194/acp-19-3257-2019

GEOPHYSICAL RESEARCH LETTERS

Supporting Information for

Contributions of World Regions to the Global Tropospheric Ozone Burden Change from 1980 to 2010

Yuqiang Zhang[1], J. Jason West[2], Louisa Emmons[3], Johannes Flemming[4,] Jan Eiof Jonson[5], Marianne Tronstad Lund[6], Takashi Sekiya[7], Kengo Sudo[7]

[1]Nicholas School of the Environment, Duke University, 9 Circuit Dr, Durham, NC 27708, USA.

[2]Environmental Sciences and Engineering Department, University of North Carolina at Chapel Hill, Chapel Hill, North Carolina 27599, USA.

[3]Atmospheric Chemistry Observations and Modeling Laboratory, National Center for Atmospheric Research (NCAR), Boulder, CO, USA

[4]European Center for Medium-Range Weather Forecasts, Reading, UK

[5]Norwegian Meteorological Institute, Oslo, Norway

[6]CICERO Center for International Climate Research, Oslo, Norway

[7]Japan Agency for Marine-Earth Science and Technology, Yokohama, Japan

[8]Nagoya University, Furocho, Chigusa-ku, Nagoya, Japan

Contents of this file

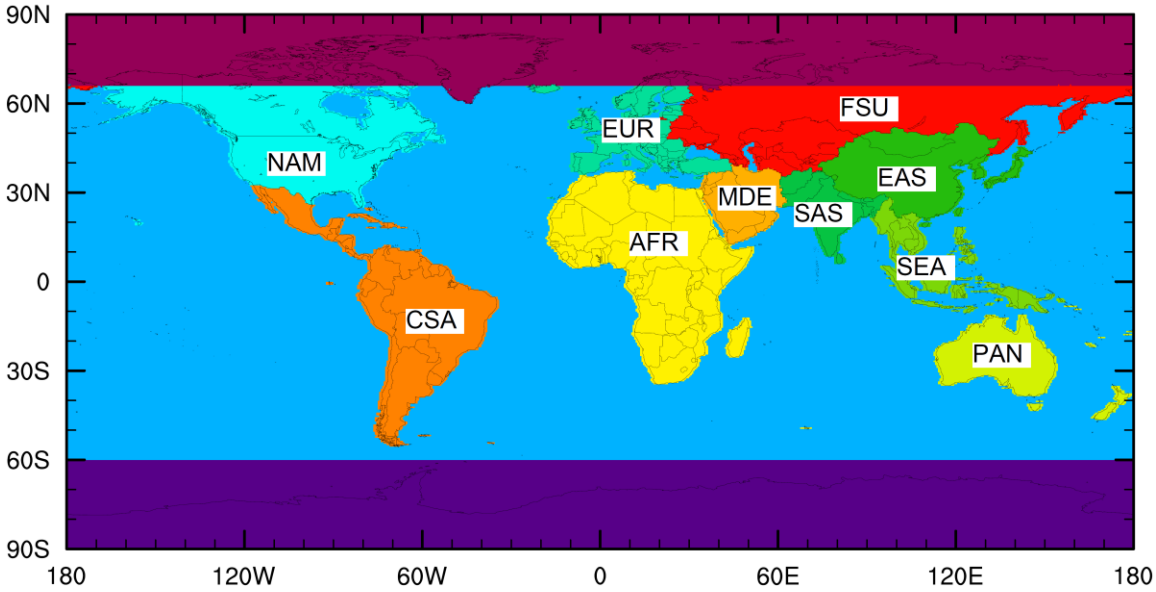

Figure S1. The 10 world regions definitions, including two extra grid cells along the coastal regions. Most of the regions are following the HTAP2 definitions (http://iek8wikis.iek.fz-juelich.de/HTAPWiki/WP2.1, last access July 2 2018), such as North America (NAM, including USA and Canada), Europe (EUR), South Asia (SAS), East Asia (EAS), South East Asia (SEA), Pacific, Australia and New Zealand (PAN), Middle East (MDE). We group Northern Africa and Sub Saharan together as new region Africa (AFR). We then group Mexico and Central America and South America together as region Central South America (CSA). We group Russia, Belarussia, Ukraine and Central Asia as region Former Soviet Union (FSU). Blue color means the Ocean region (OCN). Dark red means Arctic Circle (North of 66 N) + Greenland (NPO). Purple color means Antarctic (SPO).

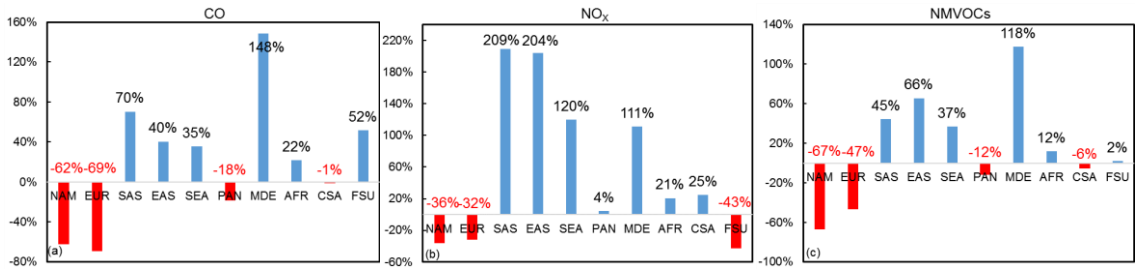

Figure S2: Percent emission changes for CO (a, (2010-1980)/1980×100%), NO_x (b), and NMVOCs (c) from 1980 to 2010 for the 10 world regions. The red color shows regions with emission decreases, and blue color shows emission increases.

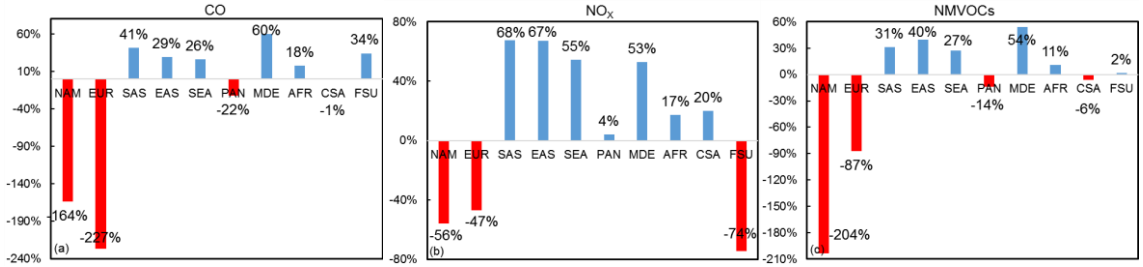

Figure S3. As for Fig. S2, but the differences are calculated as relative to the emissions totals in 2010 ((2010-1980)/2010×100%).

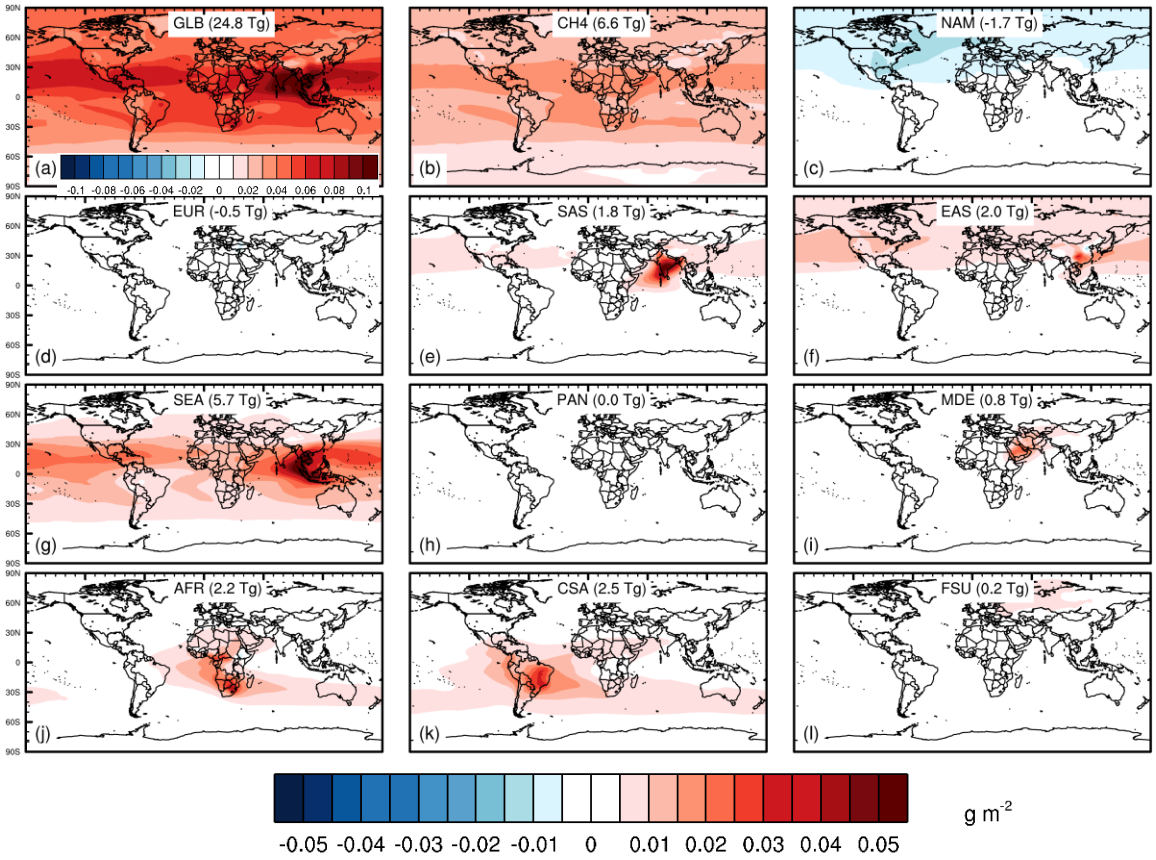

Figure S4: Spatial distributions of ΔBO_3 (g m^{-2}) from 1980 to 2010 for the season DJF, for (a) total emission changes from 1980 to 2010, (b) global CH_4 concentration change, and (c)-(l) emission changes in 10 world regions.

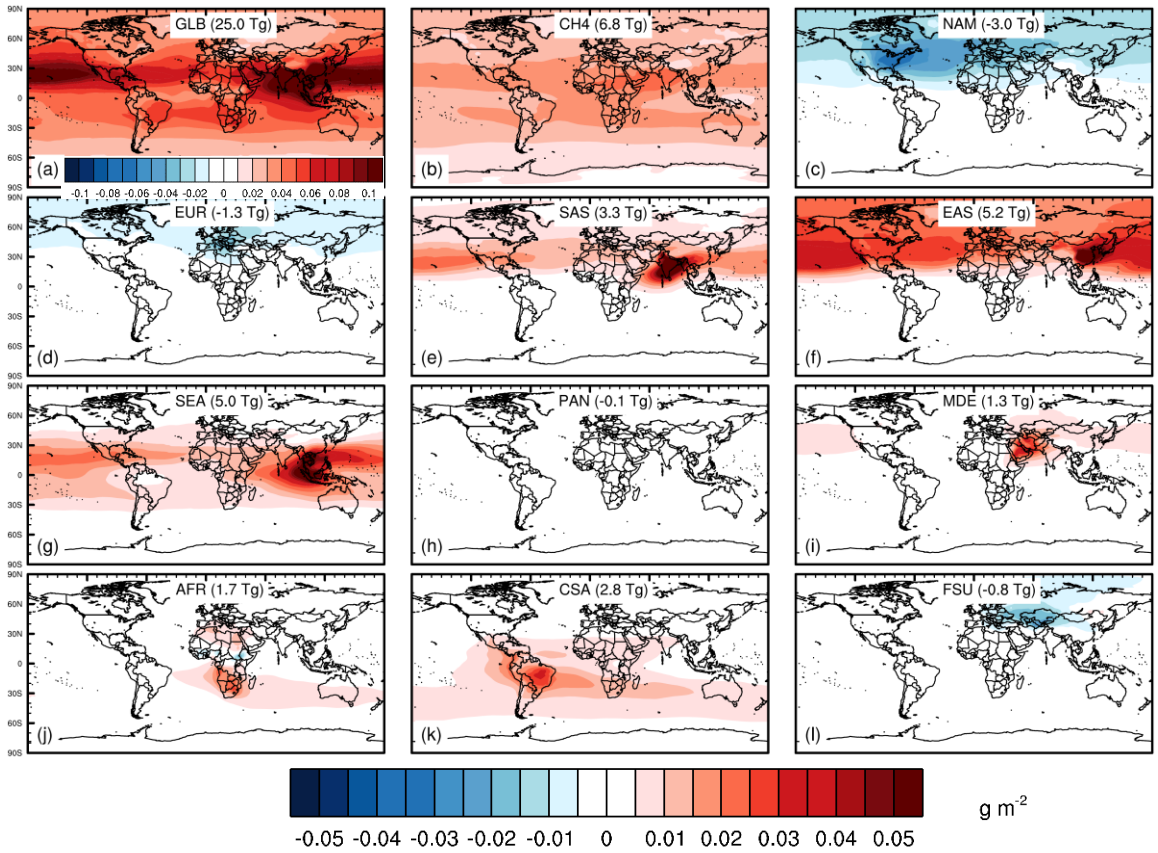

Figure S5: As in Fig. S4 but for MAM.

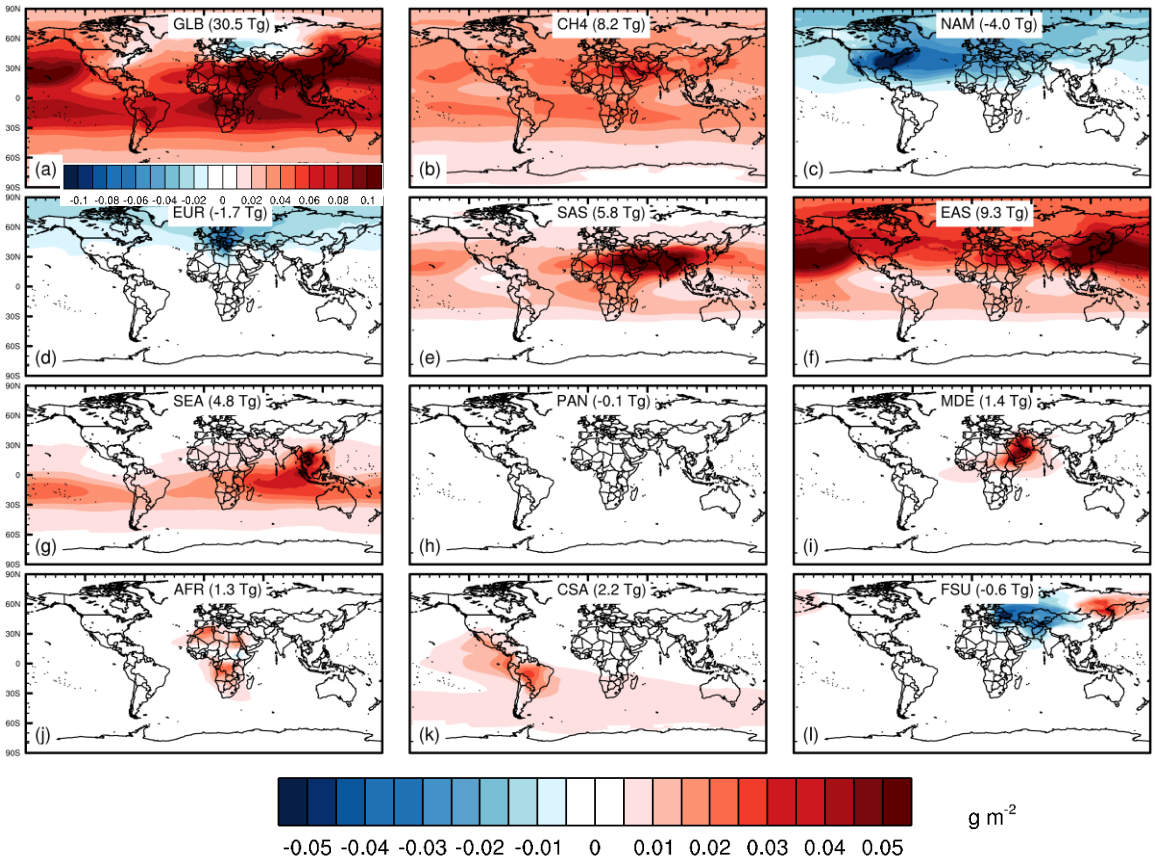

Figure S6: As in Fig. S4 but for JJA.

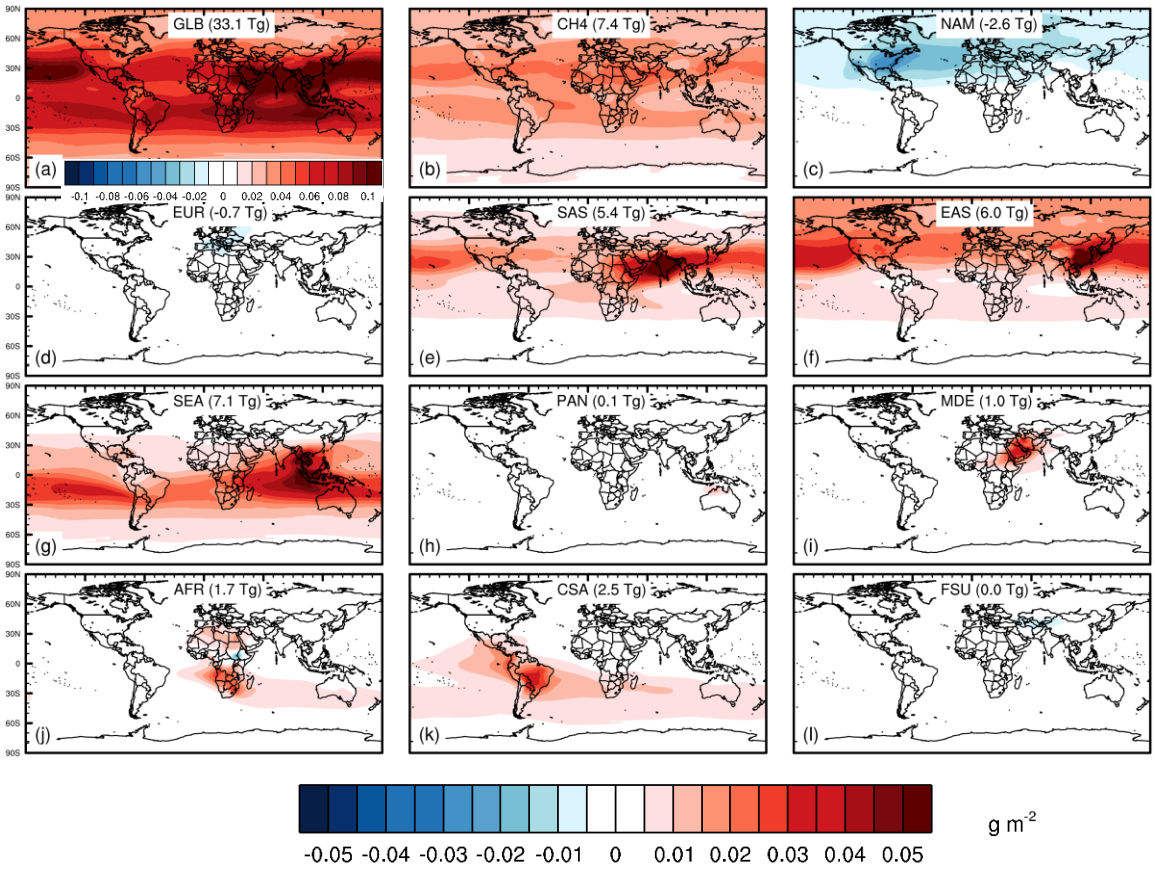

Figure S7: As in Fig. S4 but for SON.

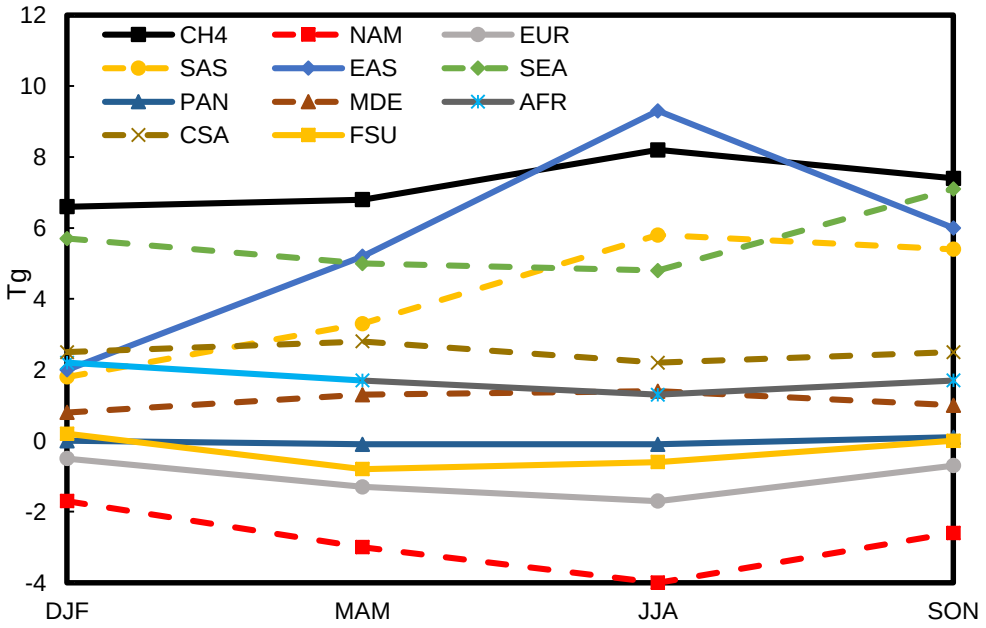

Figure S8: Seasonal distributions of the global tropospheric ozone burden changes between 1980 and 2010 from changes in the global CH_4 concentration, and regional emissions.

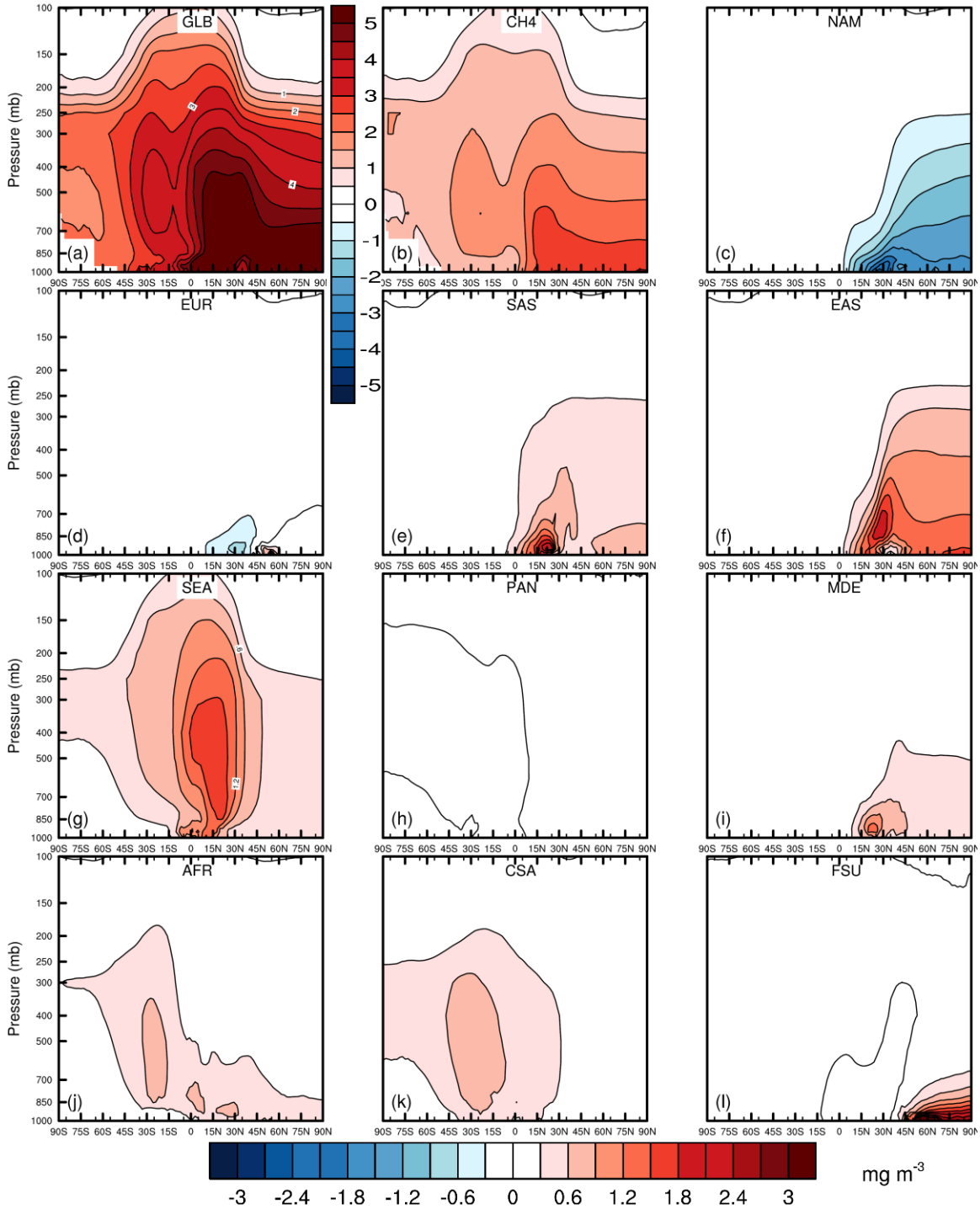

Figure S9: Zonal DJF mean O_3 change (mg m^{-3}) from 1980 to 2010, for (a) total emission changes from 1980 to 2010, (b) global CH_4 concentration change, and (c)-(l) emission changes in 10 world regions.

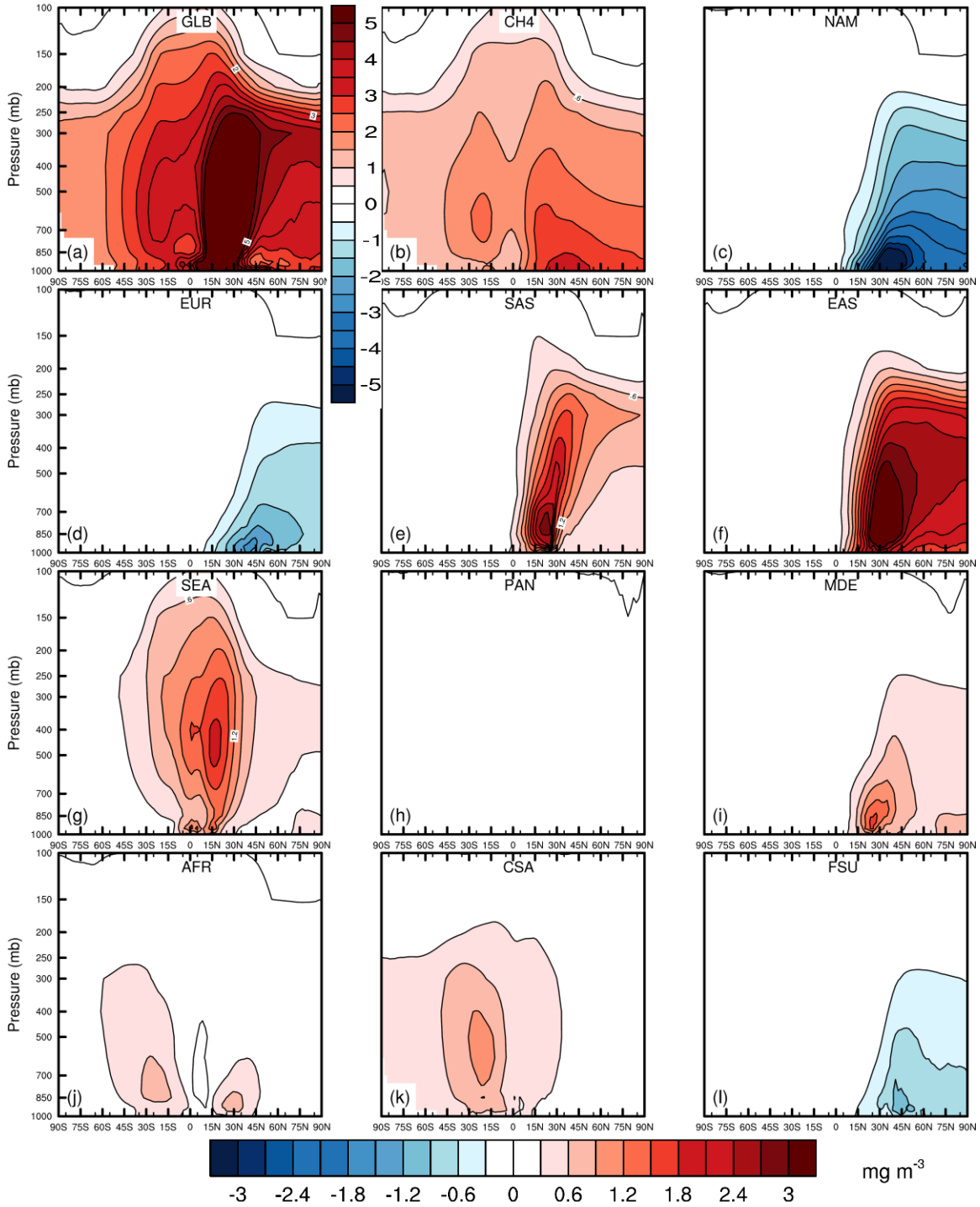

Figure S10: As in Fig. S9 but for MAM**.**

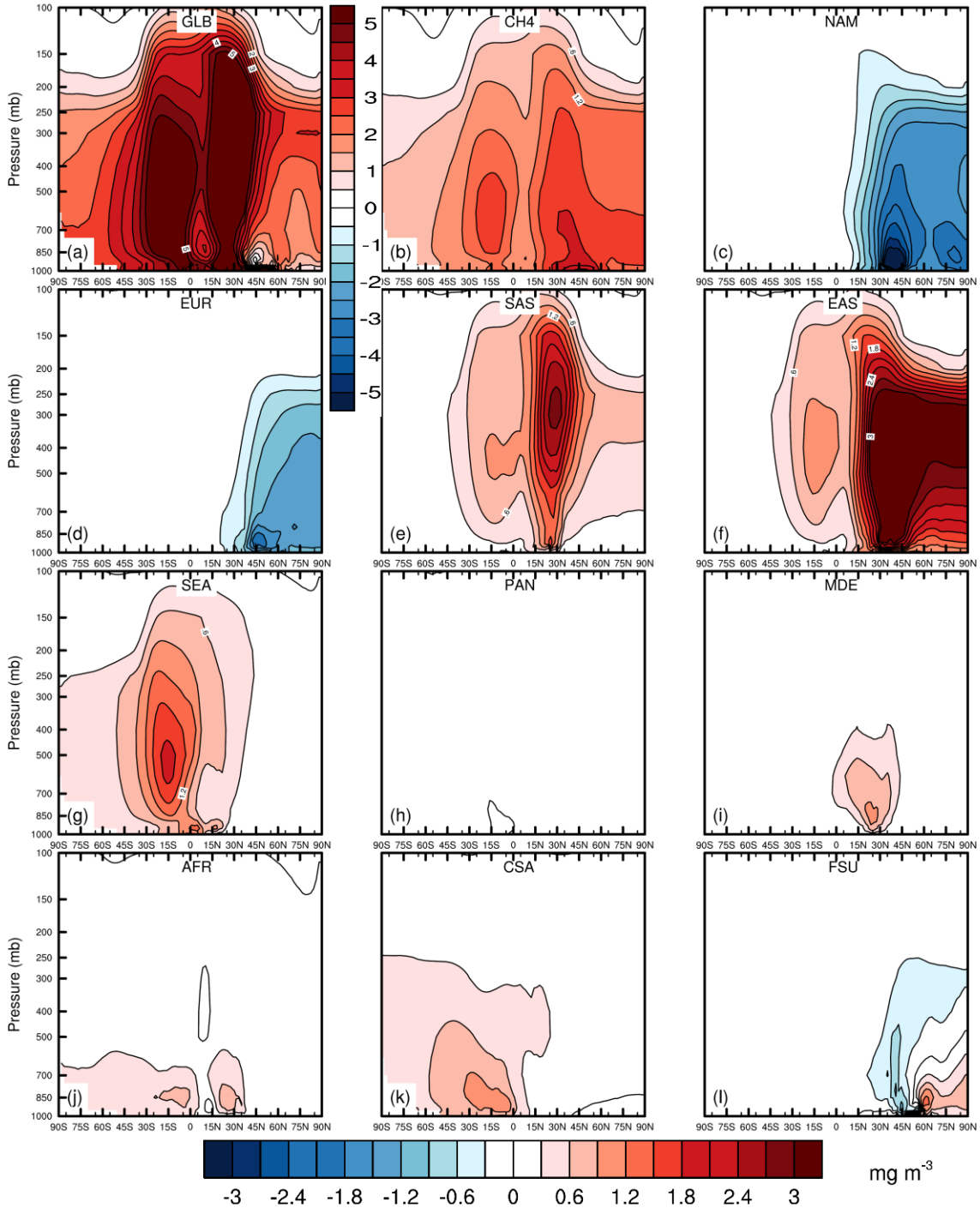

Figure S11: As in Fig. S9 but for JJA.

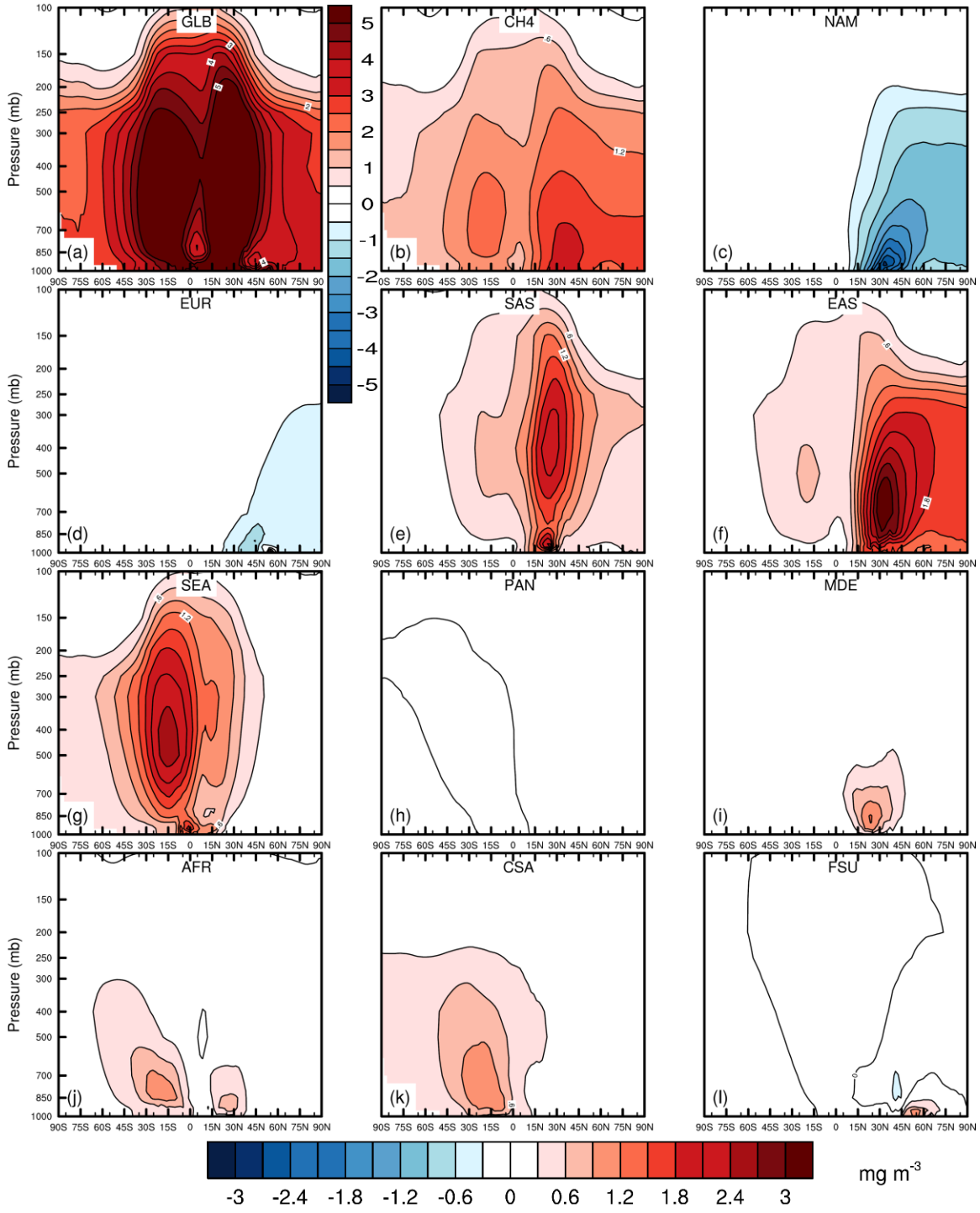
GLB
CH4
NAM
EUR
SAS
EAS
SEA
PAN
MDE
AFR
CSA
FSU
(a)
(b)
(c)
(d)
(e)
(f)
(g)
(h)
(i)
(j)
(k)
(l)
Pressure (mb)
100
150
200
250
300
400
500
700
850
1000
90S 75S 60S 45S 30S 15S 0 15N 30N 45N 60N 75N 90N
5
4
3
2
1
0
-1
-2
-3
-4
-5
-3 -2.4 -1.8 -1.2 -0.6 0 0.6 1.2 1.8 2.4 3
mg m-3

Figure S12: As in Fig. S9 but for SON.

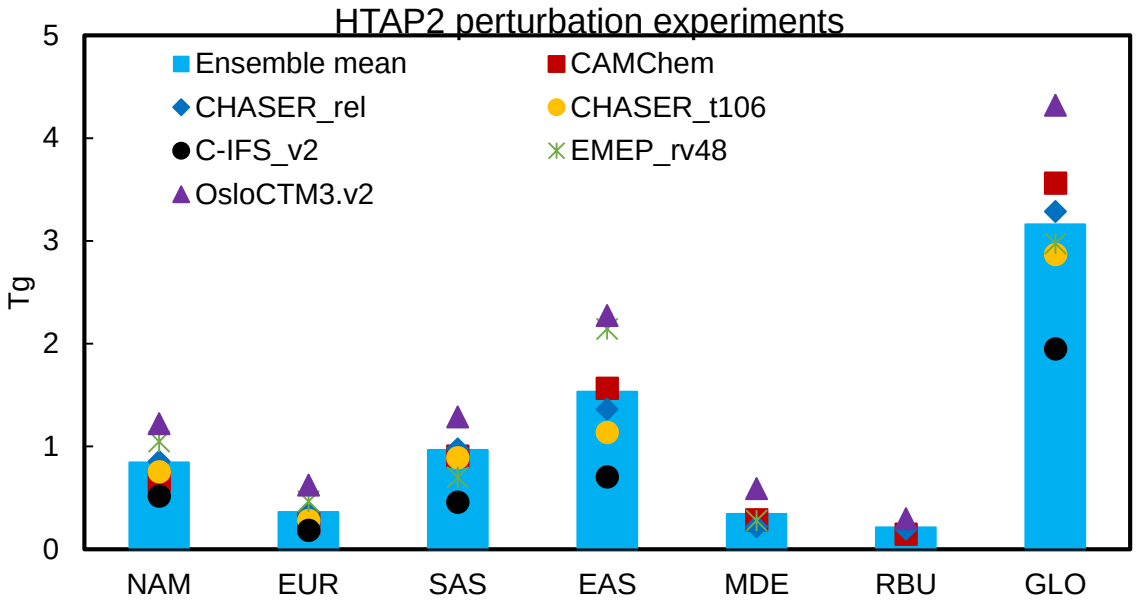

Figure S13: Global tropospheric ozone burden changes between the base and 7 perturbation experiments. The blue columns are the ensemble model mean from the 6 available models. Note that both the CHASER_t106 and C-IFS_v2 did not perform the MDE and RBU perturbation experiments, and the EMEP_rv48 model did not perform the RBU experiment. The global ozone burden changes for GLO experiments are divided by 3 for all the single and ensemble models to better fit the plot.

Table S1. Model simulations discussed in this study. The first three simulations (S_2010, S_1980, and S_CH_4) were performed in our last study (Zhang et al., 2016). The global methane concentration has increased from 1567 ppbv in 1980 to 1798 ppbv in 2010 (Prather et al., 2013).

	Anthropogenic and Biomass burning emissions in year	Global CH_4 concentration
S_2010	2010	1798 ppbv
S_1980	1980	1567 ppbv
S_CH_4	2010	1567 ppbv
S_NAM	2010 worldwide, 1980 in North America	1798 ppbv
S_EUR	2010 worldwide, 1980 in except for Europe	1798 ppbv
S_SAS	2010 worldwide, 1980 in South Asia	1798 ppbv
S_EAS	2010 worldwide, 1980 in East Asia	1798 ppbv
S_SEA	2010 worldwide, 1980 in South East Asia	1798 ppbv
S_PAN	2010 worldwide, 1980 in Pacific, Australia and New Zealand	1798 ppbv
S_MDE	2010 worldwide, 1980 in for Middle East	1798 ppbv
S_AFR	2010 worldwide, 1980 in Africa	1798 ppbv
S_CSA	2010 worldwide, 1980 in Central South America	1798 ppbv
S_FSU	2010 worldwide, 1980 in Former Soviet Union	1798 ppbv

Table S2. Regional anthropogenic emissions in 1980 and 2010 for CO, including biomass burning, and the differences in regional emissions from adding two extra grid cells. Units are Tg CO yr^{-1}. The 10 regions are defined in Figure S1.

	With 2 extra coastal grid cells			**Differences between with and without 2 extra grid cells**	
	1980	2010	Diff (Relative)	1980	2010
NAM	139.2	52.7	-86.5 (-62%)	6.0	2.0
EUR	87.4	26.8	-60.6 (-69%)	9.0	2.8
SAS	65.2	111.1	45.9 (70%)	4.0	6.6
EAS	116.2	163.2	47.0 (40%)	9.5	10.4
SEA	91.3	123.6	32.3 (35%)	18.0	24.0
PAN	25.8	21.1	-4.7 (-18%)	2.6	2.1
MDE	8.6	21.5	12.8 (148%)	0.7	1.9
AFR	228.8	278.6	49.9 (22%)	4.2	6.6
CSA	106.8	105.5	-1.2 (-1%)	5.2	5.2
FSU	42.4	64.3	21.9 (52%)	0.8	1.6
Sum[1]	911.8	968.4	56.7 (6%)	60.0	63.2
Global[2]	**967.8**	**1029.9**	**62.1 (6.4%)**		

[1]Sum are the emission totals from the 10 inland regions.

[2]Global are the emission total in all the grid cells. The differences between the Global and the Sum are the emissions over the ocean, NPO and SPO (see Figure S1).

Table S3. The same as Table S2, but for NO_x. Units are Tg NO_x yr^{-1}.

	W/ extra 2 coastal grid cells			Differences between w/ and w/o extra 2 grid cells	
	1980	2010	Diff (Relative)	1980	2010
NAM	21.2	13.6	-7.6 (-36%)	1.2	0.8
EUR	15.2	10.3	-4.8 (-32%)	1.8	1.5
SAS	2.6	8.0	5.4 (209%)	0.2	0.5
EAS	8.1	24.7	16.6 (204%)	1.1	2.1
SEA	2.5	5.5	3.0 (120%)	0.6	1.3
PAN	2.1	2.2	0.1 (4%)	0.3	0.3
MDE	2.1	4.4	2.3 (111%)	0.2	0.5
AFR	13.1	15.8	2.7 (21%)	0.4	0.7
CSA	7.1	8.8	1.8 (25%)	0.7	0.8
FSU	13.7	7.8	-5.8 (-43%)	0.3	0.2
Sum[1]	87.6	101.2	13.6 (15%)	6.9	8.6
Global[2]	**104.0**	**126.1**	**22.1 (21.2%)**		

Table S4. The same as Table S2, but for NMVOCs. Units are Tg NMVOCs yr^{-1}.

	W/ extra 2 coastal grid cells			Differences between w/ and w/o extra 2 grid cells	
	1980	2010	Diff (Relative)	1.6	0.5
NAM	24.9	8.2	-16.7 (-67%)	1.5	0.9
EUR	13.6	7.3	-6.4 (-47%)	0.4	0.6
SAS	8.3	12.0	3.7 (45%)	1.4	2.0
EAS	16.3	26.9	10.7 (66%)	3.4	4.7
SEA	16.0	22.0	6.0 (37%)	0.4	0.4
PAN	3.6	3.2	-0.4 (-12%)	0.8	1.7
MDE	6.6	14.3	7.7 (118%)	0.8	1.2
AFR	35.6	39.9	4.3 (12%)	1.4	1.3
CSA	21.3	20.1	-1.2 (-6%)	0.2	0.3
FSU	11.4	11.6	0.2 (2%)	12.1	13.6
Sum[1]	157.7	165.5	7.8 (5%)	1.6	0.5
Global[2]	**170.1**	**180.3**	**10.2 (6.0%)**		

Table S5. Available models that simulate the 20% emission perturbation experiments in global and 6 Tier 1 source regions from HTAP2, with reporting hourly O_3 at different model levels. Data are available upon request from http://aerocom.met.no, last accessed Feb 28, 2019.

Models	Institution	Contact	Model resolution (lon×lat)	Reference
CAMchem	NCAR	Louisa Emmons	2.5° × 1.9°	Tilmes et al., 2016
CHASER_rel	NAGOYA, JAMSTEC, NIES	Kengo Sudo Takashi Sekiya	2.8° × 2.8°	Sudo et al., 2002
CHASER_t106	As above	As above	1.1° × 1.1°	Sudo et al., 2002
C-IFS_v2	ECMWF	Johannes Flemming	0.7° × 0.7°	Flemming et al., 2015
EMEP_rv48	Met No	Jan Eiof Jonson	0.5° × 0.5°	Simpson et al., 2012
OsloCTM3.v2	CICERO	Marianne Tronstad Lund	2.8° × 2.8°	Søvde et al., 2012

References:

Flemming, J., Huijnen, V., Arteta, J., Bechtold, P., Beljaars, A., Blechschmidt, A.-M., et al. (2015). Tropospheric chemistry in the Integrated Forecasting System of ECMWF, Geosci. Model Dev., 8, 975–1003, https://doi.org/10.5194/gmd-8-975-2015.

Sudo, K., Takahashi, M., Kurokawa, J.-I., and Akimoto, H. (2002). CHASER: A global chemical model of the troposphere 1. Model description, J. Geophys. Res.-Atmos., 107, ACH 7-1–ACH 7-20. https://doi.org/10.1029/2001JD001113.

Tilmes, S., Lamarque, J. F., Emmons, L. K., Kinnison, D. E., Marsh, D., Garcia, R. R., et al. (2016). Representation of the Community Earth System Model (CESM1) CAM4-chem within the Chemistry-Climate Model Initiative (CCMI). *Geoscientific Model Development*, *9*(5), 1853–1890. https://doi.org/10.5194/gmd-9-1853-2016

Simpson, D., Benedictow, A., Berge, H., Bergström, R., Emberson, L. D., Fagerli, H., et al. (2012). The EMEP MSC-W chemical transport model – technical description, Atmos. Chem. Phys., 12, 7825–7865, https://doi.org/10.5194/acp-12-7825-2012.

Søvde, O. A., Prather, M. J., Isaksen, I. S. A., Berntsen, T. K., Stordal, F., Zhu, X., et al. (2012). The chemical transport model Oslo CTM3, Geosci. Model Dev., 5, 1441–1469, https://doi.org/10.5194/gmd-5-1441-2012.